Journal of Quantitative Spectroscopy & Radiative Transfer 329 (2024) 109121

Contents lists available at ScienceDirect

Journal of Quantitative Spectroscopy and Radiative Transfer

journal homepage: www.elsevier.com/locate/jqsrt

Thermal radiation at high-temperature and high-pressure conditions: Validation of HITEMP-2010 for carbon dioxide

Maximilian Dammann [a,b,c,*,1], Roman Weber [c], Alexander Fateev [d], Sønnik Clausen [d], Michael Alberti [c], Thomas Kolb [a,b], Marco Mancini [c]

[a] Karlsruhe Institute of Technology (KIT), Engler-Bunte-Institute, Fuel Technology (EBI ceb), Engler-Bunte-Ring 1, 76131 Karlsruhe, Germany
[b] Karlsruhe Institute of Technology (KIT), Institute for Technical Chemistry, Gasification Technology (ITC vgt), Hermann-von-Helmholtz-Platz 1, 76344 Eggenstein-Leopoldshafen, Germany
[c] Clausthal University of Technology, Institute for Energy Process Engineering and Fuel Technology (IEVB), Agricolastrasse 4, 38678 Clausthal-Zellerfeld, Germany
[d] Technical University of Denmark, Department of Chemical and Biochemical Engineering, CHEC Research Centre, Søltofts Plads, 2800 Kgs. Lyngby, Denmark

ARTICLE INFO

Keywords:
Radiative heat transfer
High pressure
Measurements
HITEMP-2010
Spectral transmissivity

ABSTRACT

Line-by-line models based on spectroscopic databases are powerful tools for the generation of accurate gas absorption spectra but still require validation for high-temperature and high-pressure conditions. Therefore, this study carried out spectral transmissivity measurements of CO_2/N_2 mixtures at temperatures of approximately 773 K and 1273 K and pressures between 1 bar and 60 bar. The measurement data was obtained in a spectral range from 1900 cm^{-1} to 6600 cm^{-1} at a spectral resolution of 1 cm^{-1} and was compared with line-by-line predictions. The comparisons show that the absorption spectra of CO_2 can be predicted for high-temperature and high-pressure conditions with good accuracy if the line-by-line calculations are performed using modified line profiles and the HITEMP-2010 database. In comparison with standard line-shape functions, both the Voigt line-shape function combined with the cut-off criterion of Alberti et al. (Combust. Flame 162 (2015) 597–612) and the Price line-shape function modified with one of the two ξ corrections of Westlye et al. (J. Quant. Spectrosc. Radiat. Transfer 302 (2023) 108555; J. Quant. Spectrosc. Radiat. Transfer 280 (2022) 108089) provided significantly superior predictions. However, deficiencies of the cut-off criterion of Alberti et al. become clear in the transmissivity predictions of the right wings of the 4.3 μm band and the 2.7 μm band. The Price line-shape function combined with the first ξ correction of Westlye et al. was able to overcome these erroneous predictions of the wings, while the Price line-shape function modified with the second ξ correction of Westlye et al. only proved superior for gas mixtures with 20% CO_2 and 80% N_2 (in mole fractions).

1. Introduction

High-pressure combustion and high-pressure entrained flow gasification processes are characterised by high temperatures and large partial pressures of water vapour and carbon dioxide. Mathematical modelling of both processes thus pays special attention to thermal radiation and the incorporation of appropriate thermal gas radiation property models based on accurate absorption spectra [1,2]. The latter can be obtained through spectral line-by-line calculations using the most recent available spectroscopic databases (such as HITEMP-2010 [3], CDSD-4000 [4], UCL-4000 [5] and AI-3000K [6]) and the most appropriate mathematical representation of spectral line shapes. However, validation of predictions has mainly been performed for atmospheric-pressure conditions [7–13] whereas the validation data for high-temperature and high-pressure conditions [14–20] is scarce. Furthermore, previous studies [16,21–23] have demonstrated that absorption coefficients are overestimated in the line wings while underestimated at the line centre due to deficiencies of standard line-shape functions such as the Lorentz line-shape function and the Voigt line-shape function. This has led to the development of empirical correction methods such as χ functions, line-mixing approaches and cut-off criteria.

Perin and Hartmann [16], Hartmann et al. [22], Brodbeck et al. [24] and Tran et al. [18] suggested χ functions with tabulated coefficients for specific temperature and wavenumber ranges for H_2O, CO_2 and CO. The χ functions are multiplied with the Lorentz line-shape function and correct the line wing predictions. This is usually pursued without re-scaling to preserve the line intensity, leading to increasing loss of integrated intensity with increasing pressure.

* Corresponding author.
[1] ORCID: https://orcid.org/0000-0002-2851-7787.

https://doi.org/10.1016/j.jqsrt.2024.109121
Received 4 February 2024; Received in revised form 1 July 2024; Accepted 5 July 2024
Available online 10 July 2024

Nomenclature

Latin symbols

a	function for ξ correction of Westlye et al.
b	function for ξ correction of Westlye et al.
c	speed of light
d	parameter for Voigt line-shape function
$\dot{e}$	emissive power
f	parameter for Voigt line-shape function
g	line-shape function
I	transformed intensity
k	temperature dependence coefficient
k_B	Boltzmann constant
K	absorption coefficient
L	length
m	mass
n	number of half-widths
N	number density
p	pressure
S	line intensity
T	temperature
x	mole fraction

Greek symbols

δ	pressure-shift parameter
Δ	half-width
ϵ	emissivity
η	wavenumber
τ	transmissivity
ξ	correction parameter

Subscripts and superscripts

air	for air-broadening/foreign-broadening
b	blackbody
c	centre
cold	without external blackbody radiation
D	Doppler
gas	gas
hot	with external blackbody radiation
inert	with inert gas
L	Lorentz
max	maximum
min	minimum
P	Price
self	for self-broadening
target	with target gas
V	Voigt
ϵ	with respect to the emissivity
η	spectral
τ	with respect to the transmissivity
$*$	apparent
0	reference

Acronyms

A	based on the Voigt line-shape function terminated at 5000 half-widths or below 10^{-9} cm^{-1}
AD	absolute deviation
B	based on the Voigt line-shape function combined with the cut-off criterion of Alberti et al.
C	based on the Price line-shape function terminated at 5000 half-widths or below 10^{-9} cm^{-1} and combined with the first ξ correction of Westlye et al.
D	based on the Price line-shape function terminated at 5000 half-widths or below 10^{-9} cm^{-1} and combined with the second ξ correction of Westlye et al.
DTU	Technical University of Denmark
HTPGC	high-temperature and high-pressure gas cell
LBL	line-by-line
LSF	line-shape function
RD	relative deviation
TAF	triangular apodisation function

Niro et al. [25] and Lamouroux et al. [26] developed a line-mixing approach that provides the sub-Lorentzian behaviour in the wings of the CO_2 lines at temperatures below 400 K.

Alberti et al. [21,27–31] developed cut-off criteria that provide the number of half-widths away from the line centre above which each line is to be cut [31]. The criteria were developed for H_2O, CO_2 and CO using existing measurement data [7,14,16,22,24,32,33] and omitting re-scaling to preserve the line intensity; however, the loss of integrated intensity was regarded as minor [31].

Westlye et al. [34,35] and Ren et al. [23] recently derived expressions for the ξ parameter of the Price line-shape function [36] to conserve the line intensity by accounting for super-Lorentzian behaviour at the line centre and sub-Lorentzian behaviour in line wings. Existing measurement data [15,16,18,20,22,24,32] was used to develop and test the ξ corrections for H_2O, CO_2 and CO. A first ξ correction for CO_2 [23,34] was not correlated with the CO_2 mole fraction and provided the best predictions at moderate gas temperatures and high gas pressures compared to other modifications such as cut-off criteria and χ functions. A second ξ correction for CO_2 [35] was developed as function of the CO_2 species mole fraction. The Price line-shape function combined with this ξ correction provided superior predictions for the 4.3 μm band at CO_2 mole fractions of up to 20% but was found to be less accurate and appropriate for pure CO_2 conditions.

In order to further advance the database validation and the modelling approach, this study carried out spectral transmissivity measurements of CO_2/N_2 mixtures and line-by-line (LBL) calculations following previous studies [13,20,35]. Specifically, new measurement data was compared with LBL predictions based on standard or truncated Voigt line profiles, standard or truncated Lorentz line profiles and Price line profiles combined with the first ξ correction or the second ξ correction. The methods and the results are described in Section 2 and Section 3, respectively. The conclusions are given in Section 4.

2. Methods

This section describes the methods that were applied to perform the spectral transmissivity measurements and the LBL calculations.

2.1. Spectral transmissivity measurements

Spectral transmissivity measurements were performed using the high-temperature and high-pressure gas cell (HTPGC) [20] at the Department of Chemical and Biochemical Engineering of DTU. The target

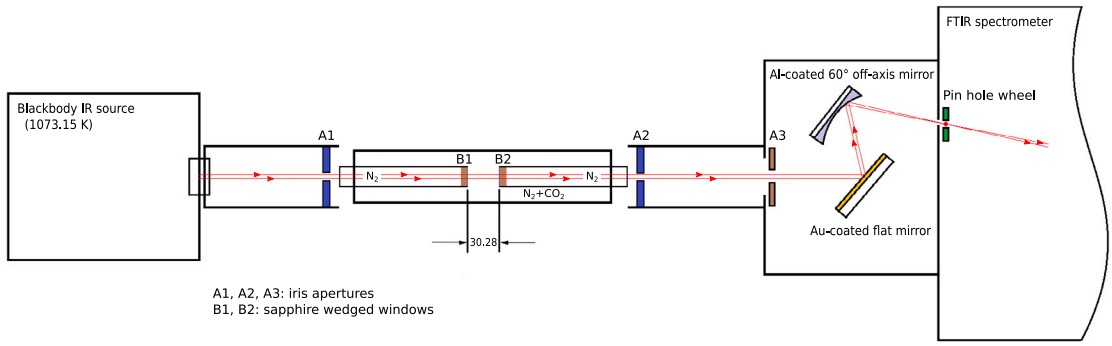

Fig. 1. Measurement set-up with high-temperature and high-pressure gas cell.

gas temperatures were 296.15 K, 773.15 K and 1273.15 K while 1 bar, 5 bar, 10 bar, 20 bar, 40 bar and 60 bar were targeted as total gas pressures. The gas cell shown in Fig. 1 has a measuring path length of 30.28 cm and consists of (i) an outer ceramic tube and two inner ceramic tubes, each made of Al_2O_3, (ii) two water-cooled brass flanges at the outer ends, (iii) two robust UV-grade sapphire windows (cut-off at 1640 cm^{-1}) and (iv) heating coils wrapped around the outer ceramic tube. Three fixed thermocouples are used as part of a heating system with three gas zones (N_2, N_2 + CO_2 and N_2) to ensure temperature uniformity over the entire measuring path length. Before the spectroscopic measurements, temperature profiles along the measuring path length inside the gas cell were measured to determine the set temperatures. Due to radiation losses, the temperature profiles changed with increasing amount of radiating gases and with increasing gas pressure. Therefore, the temperature settings were optimised to obtain uniform temperature profiles within a ±10 K accuracy for different CO_2 concentrations.

The interferograms were recorded twice using a FTIR spectrometer (Agilent Cary 660) with KBr beam splitter and InSb detector (1850–7000 cm^{-1}) and were converted to single-beam spectra with a Fast Fourier Transformation routine using a zero filling factor of 4 and the triangular apodisation function. Following previous approach [20], the apparent spectral transmissivity $\tau^*_{\eta,\mathrm{gas}}$ at a spectral resolution of 1 cm^{-1} was obtained by

$$\tau^*_{\eta,\mathrm{gas}} = \frac{I_{\mathrm{target,hot}} - I_{\mathrm{target,cold}}}{I_{\mathrm{inert,hot}} - I_{\mathrm{inert,cold}}}, \tag{1}$$

where $I_{\mathrm{target,hot}}$ is the transformed intensity from the measurement with target gas and external blackbody radiation at 1073.15 K (see Fig. 1), $I_{\mathrm{target,cold}}$ is the transformed intensity from the measurement with target gas and without external blackbody radiation (i. e. with hot gas emission from the gas cell and background radiation at ambient temperature only), $I_{\mathrm{inert,hot}}$ is the transformed intensity from the measurement with inert gas and with external blackbody radiation and $I_{\mathrm{inert,cold}}$ is the transformed intensity from the measurement with inert gas and without external blackbody radiation. N_2 (5.0, i. e. with a purity of 99.999%) were used as inert gas while CO_2 (4.8, i. e. with a purity of 99.998%) and mixtures of 20% CO_2 (4.5, i. e. with a purity of 99.995%) and 80% N_2 (5.0) were applied as target gases. The upper wavenumber limit η_{max} was between 6600 cm^{-1} and 6800 cm^{-1} while the lower limit η_{min} of approximately 1900 cm^{-1} was restricted by the cut-off of the sapphire windows and the InSb detector. Thus, the measurements focussed on the 4.3 µm band, the 2.7 µm band and the 2.0 µm band of CO_2 while measurements for the 15.0 µm band should be conducted in future studies. The conditions of the measured spectra are summarised in Table 1.

The interferograms were slightly affected by ice formation on the inner surface of the window of the InSb detector due to vacuum conditions. As the ice developed with increasing time and the impact of ice and H_2O could be identified in the measured data due to the local well-defined broad/sharp structures, the erroneous signals were removed from the flawed apparent transmissivity spectra.

Table 1
Conditions of the measured spectra: mixture, gas temperature T_{gas}, gas pressure p_{gas}, minimum wavenumber η_{min} and maximum wavenumber η_{max}.

	Mixture	$\frac{T_{\mathrm{gas}}}{\mathrm{K}}$	$\frac{p_{\mathrm{gas}}}{\mathrm{bar}}$	$\frac{\eta_{\mathrm{min}}}{\mathrm{cm^{-1}}}$	$\frac{\eta_{\mathrm{max}}}{\mathrm{cm^{-1}}}$
1	100% CO_2	296.75	1.02	1900	6600
2	20% CO_2 + 80% N_2	784.25	1.05	1900	6800
3	20% CO_2 + 80% N_2	783.25	5.03	1900	6800
4	20% CO_2 + 80% N_2	781.35	10.30	1900	6800
5	20% CO_2 + 80% N_2	777.15	20.26	1900	6800
6	20% CO_2 + 80% N_2	772.25	40.05	1900	6800
7	20% CO_2 + 80% N_2	773.15	60.22	1900	6740
8	20% CO_2 + 80% N_2	1281.54	1.04	1900	6800
9	20% CO_2 + 80% N_2	1280.67	5.03	1900	6800
10	20% CO_2 + 80% N_2	1276.01	10.00	1900	6800
11	20% CO_2 + 80% N_2	1275.82	19.96	1900	6800
12	20% CO_2 + 80% N_2	1265.92	40.00	1900	6800
13	20% CO_2 + 80% N_2	1280.57	54.14	1900	6600
14	100% CO_2	780.15	1.01	1900	6800
15	100% CO_2	780.15	5.13	1900	6800
16	100% CO_2	779.63	10.27	1900	6800
17	100% CO_2	771.39	20.27	1900	6800
18	100% CO_2	775.56	40.14	1900	6800
19	100% CO_2	1281.54	1.02	1900	6600
20	100% CO_2	1280.67	5.025	1900	6600
21	100% CO_2	1276.01	10.00	1900	6600
22	100% CO_2	1276.01	20.00	1900	6600
23	100% CO_2	1265.92	40.00	1900	6600

2.2. LBL calculations

LBL calculations were carried out using the HITEMP-2010 database for CO_2 [3] and the LBL software of Alberti et al. [21,27,28,30,31]. The HITEMP-2010 database provided the parameters for the calculation of the absorption lines of CO_2 at the reference pressure p_0 = 1 atm and the reference temperature T_0 = 296 K, including the vacuum centre wavenumbers $\eta_{\mathrm{c},0}$, the reference integrated line intensities S_0, the pressure-shift parameters δ, the reference half-widths for self-broadening $\Delta_{\mathrm{self},0}$, the reference half-widths for air-broadening[2] $\Delta_{\mathrm{air},0}$ and the dimensionless temperature dependence coefficients k. The LBL software enabled the calculation of the gas absorption spectra at the measured gas conditions between a minimum wavenumber η_{min} = 0 and a maximum wavenumber η_{max} < 15 000 cm^{-1} with a wavenumber step size of 0.01 cm^{-1}. The gas absorption spectra were obtained through summation of the absorption contributions of all lines, i. e. the spectral gas absorption coefficient $K_{\eta,\mathrm{gas}}$ was determined by

$$K_{\eta,\mathrm{gas}}(\eta) = \sum_{i=1}^{11193608} K_{\eta,i}(\eta)\,, \tag{2}$$

[2] Air-broadening parameters instead of N_2-broadening parameters results in negligible differences in line intensities based on the experience of the authors.

where $K_{\eta,i}$ is the spectral absorption coefficient K_η of line i. The spectral absorption coefficient K_η of a line is described by

$$K_\eta\left(\eta, p_{\text{gas}}, T_{\text{gas}}, x_{\text{CO}_2,\text{gas}}\right) = S\left(T_{\text{gas}}\right)\, N\left(p_{\text{gas}}, T_{\text{gas}}, x_{\text{CO}_2,\text{gas}}\right)\, g\left(\eta-\eta_{\text{c}}, p_{\text{gas}}, T_{\text{gas}}, x_{\text{CO}_2,\text{gas}}\right), \tag{3}$$

where S is the temperature-scaled line intensity based on the reference line intensity S_0, N is the number density based on the ideal gas equation of state, g is the line-shape function as function of the centre wavenumber $\eta_{\text{c}} = \eta_{\text{c},0} + \delta\, p_{\text{gas}}$, p_{gas} is the gas pressure, T_{gas} is the gas temperature and $x_{\text{CO}_2,\text{gas}}$ is the gas species mole fraction of CO_2. Three line-shape functions were applied in this study: the Lorentz line-shape function g_{L}, the Price line-shape function g_{P} and the Voigt line-shape function g_{V}. The Lorentz line-shape function g_{L} is defined by

$$g_{\text{L}} = \frac{1}{\pi\,\Delta_{\text{L}}}\left(1+\left(\frac{\eta-\eta_{\text{c}}}{\Delta_{\text{L}}}\right)^2\right)^{-1}, \tag{4}$$

where

$$\Delta_{\text{L}} = \left(p_{\text{CO}_2,\text{gas}}\,\Delta_{\text{self},0} + \left(p_{\text{gas}} - p_{\text{CO}_2,\text{gas}}\right)\,\Delta_{\text{air},0}\right)\left(\frac{T_0}{T_{\text{gas}}}\right)^k \tag{5}$$

is the simplified expression for the Lorentz half-width taking into account both self-broadening and foreign-broadening. The Price line-shape function g_{P} is given by

$$g_{\text{P}} = \frac{\xi\,\sin(\pi/\xi)}{2\,\pi\,\Delta_{\text{L}}}\left(1+\left|\frac{\eta-\eta_{\text{c}}}{\Delta_{\text{L}}}\right|^{\xi}\right)^{-1}, \tag{6}$$

where $\xi = \xi\left(p_{\text{gas}}, T_{\text{gas}}, x_{\text{CO}_2,\text{gas}}\right)$ is a line-shape correction parameter. Recently, Westlye et al. suggested two possible approaches. The first approach is given by [23,34]

$$\xi = \begin{cases} 2+\left(\mathrm{e}^{-1}-\exp\left(-\left(\dfrac{p_{\text{gas}}}{1\,\text{bar}}\right)^{0.1}\right)\right)\,b\left(T_{\text{gas}}\right), & \text{if } p_{\text{gas}} \geq 1\,\text{bar} \\ 2, & \text{else} \end{cases}, \tag{7}$$

where $b\left(T_{\text{gas}}\right) = \left(632.19\,\text{K}/T_{\text{gas}}\right)^{3.48} + 6.98$. The second approach is defined by [35]

$$\xi = 2 + a\left(p_{\text{gas}}\right)\,b\left(T_{\text{gas}}\right)\left(1-x_{\text{CO}_2,\text{gas}}\right), \tag{8}$$

where $a\left(p_{\text{gas}}\right) = \exp\left(1-\left(p_0/p_{\text{gas}}\right)^{0.1}\right)$ and $b\left(T_{\text{gas}}\right) = 3.66\,\left(T_0/T_{\text{gas}}\right)^{0.23}$. The Voigt line-shape function g_{V}, which also accounts for Doppler broadening, is described by

$$g_{\text{V}} = \frac{d\,\sqrt{\ln(2)}}{\pi^{3/2}\,\Delta_{\text{D}}}\int_{-\infty}^{\infty}\frac{\exp\left(-y^2\right)}{d^2+\left(f-y^2\right)}\,\mathrm{d}y, \tag{9}$$

where $d = \sqrt{\ln(2)}\,\Delta_{\text{L}}/\Delta_{\text{D}}$ and $f = \sqrt{\ln(2)}\,\left(\eta-\eta_{\text{c}}\right)/\Delta_{\text{D}}$ are parameters and

$$\Delta_{\text{D}} = \frac{\eta_{\text{c}}}{c}\sqrt{\frac{2\,k_{\text{B}}\,T_{\text{gas}}}{m}\,\ln(2)} \tag{10}$$

is the expression for the Doppler half-width with c for the speed of light, k_{B} for the Boltzmann constant and m for the mass of the molecule.

The line-shape functions asymptotically approach zero. The *infinitely* long lines were therefore truncated in the wings. Specifically, as extending the lines below $10^{-9}\,\text{cm}^{-1}$ or beyond 5000 half-widths brings minor changes to the line and the spectrum absorptance, the lines were terminated when the absorption coefficient was below $10^{-9}\,\text{cm}^{-1}$ or the distance to the line centre exceeded 5000 half-widths. As another approach, lines based on the Lorentz line-shape function or the Voigt line-shape function were cut at n half-widths based on the empirical cut-off criterion of Alberti et al. [31]

$$n(p_{\text{gas}}, T_{\text{gas}}) = 429.99\cdot\left(\frac{T_{\text{gas}}}{296\,\text{K}}\,\frac{1\,\text{bar}}{p_{\text{gas}}}\right)^{0.822}. \tag{11}$$

2.2.1. Line-shape deficiencies

Corrections to line-shape functions either through the approaches of Westlye et al. [23,34,35] or through the cut-off criterion of Alberti et al. [31] are ad-hoc modifications derived to match the calculated transmissivities with the measured ones and to heal the deficiencies of the standard line-shape functions.

Several new functions have recently been introduced and tested in order to provide a sub-percent accuracy in the mathematical description of a single absorption line [37]. However, these new functions require a high number of additional line-shape parameters [37] and may be considered in future studies.

2.2.2. Line-mixing effects

Single absorption lines cannot be regarded as collisionally isolated one from another when collisions between molecules are numerous. Thus, line-mixing effects occur [37,38] between clusters of lines. The line-mixing affects absorption coefficients close to the centre of the cluster when radiator-perturber interactions permit efficient population exchange between the lower and the upper energy levels. This results in an enhanced absorption in a narrower region at the cluster centre and a weaker absorption in the cluster wings.

Several approaches [38,39] have been developed to account for line mixing as it is important for CO_2 absorption in the Earth's atmosphere [37]. Furthermore, it is apparent that the line-mixing effects increase with increasing density. Thus, line-mixing effects are expected to be pronounced for most of the conditions listed in Table 1. Specifically, the line-mixing effects could be significant for the cluster wings as most of the line-clusters are saturated at the cluster centre. However, the approaches are for low-temperature conditions only, while no general methods are currently available for high-temperature and high-pressure conditions since the problem is complex. Therefore, these effects were not accounted for in the LBL calculations of this study.

2.2.3. Comparisons

For the CO_2 line at $2125.000030\,\text{cm}^{-1}$, 773.15 K and 60 bar in 20% CO_2 and 80% N_2, four line profiles are compared in Fig. 2: (A) the standard Voigt profile terminated at 5000 half-widths (which completely overlaps with the standard Lorentz profile), (B) the Voigt profile terminated at 33 half-widths based on the cut-off criterion of Alberti et al. [21] (which completely overlaps with the truncated Lorentz profile), (C) the Price profile terminated at 5000 half-widths and $\xi = 2.99$ based on the first ξ correction of Westlye et al. [23,34] and (D) the Price profile terminated at 5000 half-widths and $\xi = 2.85$ based on the second ξ correction of Westlye et al. [35]. The Price profiles suggest lower absorption in the line wings and higher absorption at the line centre compared to the Lorentz and Voigt profiles and may provide a superior mathematical line representation, recalling that both Lorentz and Voigt profiles overestimate the absorption in the line wings. However, the overestimation is typically reduced when Lorentz and Voigt profiles are truncated using the cut-off criterion of Alberti et al. [31].

2.3. Transmissivities and emissivities

Predicted apparent spectral transmissivity and predicted apparent spectral emissivity spectra were determined through convolution of the calculated gas transmissivity spectrum with the Fourier transform of the triangular apodisation function used for the single beam spectra calculations from the measured interferograms (see Section 2.1). The convolution was performed to enable a comparison with the measurement data at the spectral resolution of $1\,\text{cm}^{-1}$ (see [13,35]). The apparent spectral gas transmissivity $\tau^*_{\eta,\text{gas}}$ and the apparent spectral gas emissivity $\varepsilon^*_{\eta,\text{gas}}$ are given by

$$\tau^*_{\eta,\text{gas}} = \exp\left(-K_{\eta,\text{gas}}\,L\right) * \mathcal{F}\,\text{TAF}, \tag{12}$$

$$\varepsilon^*_{\eta,\text{gas}} = 1-\tau^*_{\eta,\text{gas}}, \tag{13}$$

Table 2
Minimum wavenumbers η_{min} and maximum wavenumbers η_{max} used for the calculation of the apparent total gas emissivities and the apparent band gas emissivities.

Gas emissivity	$\frac{\eta_{min}}{cm^{-1}}$	$\frac{\eta_{max}}{cm^{-1}}$
Total	1900	6600
4.3 μm band	1800	2700
2.7 μm band	3200	4000
2.0 μm band	4600	5400

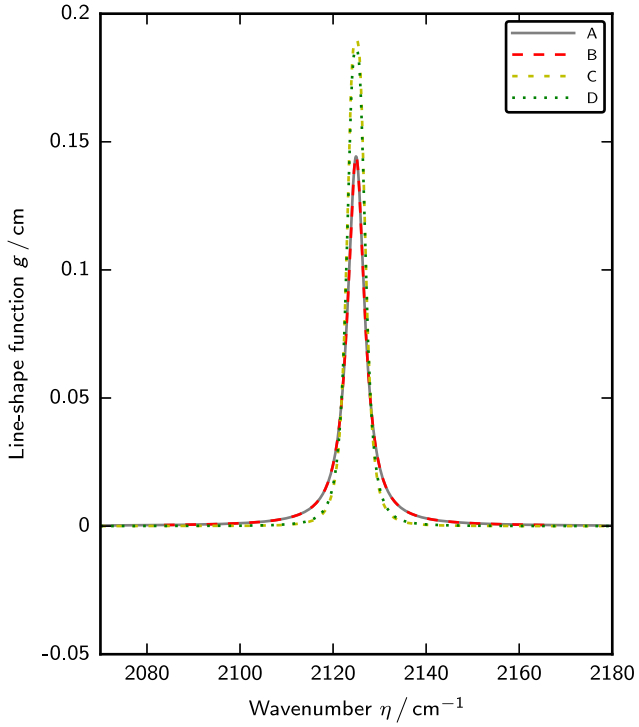

Fig. 2. Voigt and Price line profiles for CO_2 line at 2125.000030 cm^{-1}, 773.15 K and 60 bar in 20% CO_2 and 80% N_2. For details of legend, see list of acronyms.

where $K_{\eta,gas}$ is the spectral gas absorption coefficient, L is the path length and $\mathcal{F}\,TAF = sinc^2\left(\eta/cm^{-1}\right)\ cm^{-1}$ is the Fourier transform of the triangular apodisation function (i. e. the instrument line-shape function with an instrument resolution of 1 cm^{-1}). The apparent band gas emissivities or the apparent total gas emissivities ε^*_{gas} were calculated by

$$\varepsilon^*_{gas} = \frac{\int_{\eta_{min}}^{\eta_{max}} \varepsilon^*_{\eta,gas}\, \dot{e}_{\eta,b}\,(\eta,T)\ d\eta}{\int_{\eta_{min}}^{\eta_{max}} \dot{e}_{\eta,b}\,(\eta,T)\ d\eta}\,, \tag{14}$$

where η_{min} and η_{max} are the minimum and the maximum wavenumbers for the respective apparent band gas emissivity or the apparent total gas emissivity and $\dot{e}_{\eta,b}$ is the Planck function. Apparent total gas emissivities and apparent band gas emissivities for the 4.3 μm band, the 2.7 μm band and the 2.0 μm band were determined using the minimum wavenumbers η_{min} and the maximum wavenumbers η_{max} given in Table 2.

2.4. Absolute and relative deviations

Results of the transmissivity measurements and the LBL calculations are compared using absolute deviations (AD) and relative deviations (RD) which are given by

$$AD_\tau = \tau^*_{\eta,gas}\Big|_{LBL} - \tau^*_{\eta,gas}\Big|_{HTPGC}\,, \tag{15}$$

$$RD_\varepsilon = \frac{\varepsilon^*_{gas}\Big|_{LBL} - \varepsilon^*_{gas}\Big|_{HTPGC}}{\varepsilon^*_{gas}\Big|_{HTPGC}}\,, \tag{16}$$

where LBL refers to the LBL calculations and HTPGC refers to the transmissivity measurements.

3. Results

This section presents the results of the transmissivity measurements and the LBL calculations, while the measured transmissivity spectra are provided in the Supplementary material.

3.1. Transmissivity spectra

Measured and predicted apparent transmissivity spectra are compared in Figs. 3–25 (each on the left side). The predicted spectra were obtained using (A) the standard Voigt line-shape function terminated at 5000 half-widths or below $10^{-9}\ cm^{-1}$ (*infinitely* long), (B) the Voigt line-shape function combined with the cut-off criterion of Alberti et al. [21] and (C) the Price line-shape function terminated at 5000 half-widths or below $10^{-9}\ cm^{-1}$ (*infinitely* long) and combined with the first ξ correction of Westlye et al. [23,34]. The comparisons show that the measured spectra can be well predicted if the cut-off approach is applied or the first ξ correction is incorporated into the Price line-shape function. Furthermore, for high-temperature and high-pressure conditions (for example, see Fig. 8 (left; condition 6) and Fig. 25 (left; condition 23)), the Price line-shape function with the first ξ correction is typically superior to the Voigt line-shape function combined with the cut-off criterion as the cut-off approach has deficiencies in the predictions of the right wings of the 4.3 μm band and the 2.7 μm band. Absolute local deviations in small wavenumber ranges can be larger than 0.6 in the case of the right wing of the 4.3 μm band. In contrast, for atmospheric-pressure conditions (see Fig. 3 (left; condition 1)), the measured spectrum is in good agreement with the spectrum calculated using the Voigt line-shape function and the cut-off criterion, while the standard Voigt line-shape function and the Price line-shape function with the first ξ correction of Westlye et al. [23,34] underpredict the right wing of the 4.3 μm band.

3.2. Emissivities

Measured and predicted apparent total gas emissivities and measured and predicted apparent band gas emissivities are shown alongside the relative deviations in Figs. 3–25 (each on the right side). The predicted emissivities were obtained using (A) the standard Voigt line-shape function terminated at 5000 half-widths or below $10^{-9}\ cm^{-1}$ (*infinitely* long), (B) the Voigt line-shape function applied with the cut-off criterion of Alberti et al. [21] and (C) the Price line-shape function terminated at 5000 half-widths or below $10^{-9}\ cm^{-1}$ (*infinitely* long) and combined with the first ξ correction of Westlye et al. [23,34].

3.2.1. Voigt line-shape function with cut-off criterion

The apparent total gas emissivities are predicted well using the Voigt line-shape function and the cut-off criterion of Alberti et al. [21] (for example, see Fig. 8 (right; condition 6) and Fig. 25 (right; condition 23)). The absolute relative deviations for the apparent total gas emissivities are always below 11% and mainly below 5% (see results for line-shape function B in Table 3). Realising that the cut-off criterion was developed to obtain reliable overall results, this is again reflected in the accuracy of the predicted apparent total gas emissivities. Some larger absolute relative deviations can be found for the apparent band gas emissivities in Tables 4–6 (see results for line-shape function B). For the 2.0 μm band, this is mainly due to the low absolute values of the band gas emissivities. For the 2.7 μm band and the 4.3 μm band, this is due to the erroneous predictions of the right wings, where the errors are larger for the 4.3 μm band than for the 2.7 μm band. The LBL model

Table 3
Relative deviations concerning the apparent total gas emissivities of CO_2 based on the LBL model with the HITEMP-2010 database and three line-shape functions. B: Voigt line-shape function with the cut-off criterion of Alberti et al. [21], C: Price line-shape function with the first ξ correction of Westlye et al. [23,34], D: Price line-shape function with the second ξ correction of Westlye et al. [35].

LSF	$x_{CO_2,gas}$	T_{gas} / K	RD_ε / %					
			1 bar	5 bar	10 bar	20 bar	40 bar	60 bar
B	0.2	773.15	−2.02	0.80	1.29	5.32	8.74	10.82
		1273.15	−3.94	−0.93	−0.73	0.26	2.64	−3.77
	1.0	773.15	−3.14	1.98	4.67	7.54	6.87	–
		1273.15	−1.80	0.10	0.32	3.00	6.11	–
C	0.2	773.15	−2.10	0.09	−0.74	0.01	−0.48	0.72
		1273.15	−4.06	−1.25	−1.20	−1.13	−0.88	−0.75
	1.0	773.15	−2.73	−0.03	−0.38	−0.45	−0.08	–
		1273.15	−1.77	−0.48	−1.13	−0.38	0.48	–
D	0.2	773.15	−2.02	0.24	−0.48	0.60	0.97	3.10
		1273.15	−4.01	−1.16	−1.11	−0.94	−0.41	−0.08
	1.0	773.15	−2.73	9.43	26.11	63.70	122.45	–
		1273.15	−1.75	1.67	4.93	16.11	40.37	–

Table 4
Relative deviations concerning the apparent band gas emissivities of the 4.3 µm band of CO_2 based on the LBL model with the HITEMP-2010 database and three line-shape functions. B: Voigt line-shape function with the cut-off criterion of Alberti et al. [21], C: Price line-shape function with the first ξ correction of Westlye et al. [23,34], D: Price line-shape function with the second ξ correction of Westlye et al. [35].

LSF	$x_{CO_2,gas}$	T_{gas} / K	RD_ε / %					
			1 bar	5 bar	10 bar	20 bar	40 bar	60 bar
B	0.2	773.15	−1.47	1.53	2.91	7.92	12.64	14.24
		1273.15	−1.79	0.61	0.91	2.77	6.89	9.60
	1.0	773.15	−1.37	3.27	7.16	10.48	8.48	–
		1273.15	−0.50	1.92	2.73	6.62	10.86	–
C	0.2	773.15	−1.55	0.83	0.48	0.98	0.30	0.95
		1273.15	−1.93	0.23	0.24	0.44	0.46	1.07
	1.0	773.15	−0.90	1.02	0.28	−0.34	−0.13	–
		1273.15	−0.45	1.25	0.18	0.04	0.29	–
D	0.2	773.15	−1.47	0.97	0.77	1.72	2.20	4.11
		1273.15	−1.87	0.33	0.35	0.72	1.25	2.29
	1.0	773.15	−0.90	12.16	33.17	75.14	126.00	–
		1273.15	−0.42	4.20	9.91	27.15	60.28	–

Table 5
Relative deviations concerning the apparent band gas emissivities of the 2.7 µm band of CO_2 based on the LBL model with the HITEMP-2010 database and three line-shape functions. B: Voigt line-shape function with the cut-off criterion of Alberti et al. [21], C: Price line-shape function with the first ξ correction of Westlye et al. [23,34], D: Price line-shape function with the second ξ correction of Westlye et al. [35].

LSF	$x_{CO_2,gas}$	T_{gas} / K	RD_ε / %					
			1 bar	5 bar	10 bar	20 bar	40 bar	60 bar
B	0.2	773.15	−11.00	−3.51	−4.43	−2.35	−0.81	2.32
		1273.15	−18.15	−5.09	−3.87	−3.50	−2.30	−2.35
	1.0	773.15	−13.40	−1.52	−1.07	0.74	3.39	–
		1273.15	−7.72	−2.72	−2.35	−0.64	1.51	–
C	0.2	773.15	−11.04	−4.35	−4.78	−2.61	−1.89	0.26
		1273.15	−18.16	−5.19	−3.84	−3.35	−2.33	−2.62
	1.0	773.15	−13.39	−2.95	−1.77	−0.48	0.01	–
		1273.15	−7.27	−3.19	−2.59	−0.98	0.28	–
D	0.2	773.15	−11.01	−4.20	−4.70	−2.56	−1.79	0.42
		1273.15	−18.16	−5.14	−3.81	−3.30	−2.30	−2.57
	1.0	773.15	−13.39	−1.05	0.38	5.31	17.50	–
		1273.15	−7.25	−2.60	−1.90	0.62	5.39	–

Table 6
Relative deviations concerning the apparent band gas emissivities of the 2.0 µm band of CO_2 based on the LBL model with the HITEMP-2010 database and three line-shape functions. B: Voigt line-shape function with the cut-off criterion of Alberti et al. [21], C: Price line-shape function with the first ξ correction of Westlye et al. [23,34], D: Price line-shape function with the second ξ correction of Westlye et al. [35].

LSF	$x_{CO_2,gas}$	T_{gas} / K	RD_ε / %					
			1 bar	5 bar	10 bar	20 bar	40 bar	60 bar
B	0.2	773.15	−40.60	−10.71	−2.75	−6.99	−4.31	−5.84
		1273.15	−44.80	−17.95	−17.42	−5.84	−3.13	−9.43
	1.0	773.15	−26.53	−3.09	−5.77	−3.26	−2.09	–
		1273.15	9.67	0.54	−4.52	−1.61	−1.13	–
C	0.2	773.15	−40.59	−10.47	−2.28	−6.24	−3.04	−4.17
		1273.15	−44.80	−17.64	−17.01	−5.18	−2.10	−8.26
	1.0	773.15	−26.51	−2.92	−5.40	−2.63	−1.22	–
		1273.15	9.67	0.76	−4.19	−1.07	−0.28	–
D	0.2	773.15	−40.59	−10.48	−2.29	−6.24	−3.03	−4.16
		1273.15	−44.81	−17.68	−17.04	−5.21	−2.13	−8.28
	1.0	773.15	−26.51	−2.83	−4.31	3.20	10.97	–
		1273.15	9.67	0.60	−4.28	−0.61	4.37	–

with the cut-off criterion can only roughly compensate the imperfect Voigt line-shape function.

Cutting the line profiles leads to losses of integrated intensity compared to the analytical intensity. However, the absolute errors are mainly less than 1% for predictions using the Voigt line-shape function and the cut-off criterion of Alberti et al. [21] as shown in Table 7. This is in agreement with previous observations [31,38].

3.2.2. Price line-shape function with first ξ correction

The apparent total gas and the apparent band gas emissivities are also predicted quite well using the Price line-shape function and the first ξ correction of Westlye et al. [23,34] (for example, see Fig. 8 (right; condition 6) and Fig. 25 (right; condition 23). This is also evident from the relative deviations given in Tables 3–6 (see results for line-shape function C). Blue-coloured values indicate that the absolute relative deviations are smaller than corresponding values based on the Voigt line-shape function and the cut-off criterion of Alberti et al. [21], while brown-coloured values mean that the absolute relative deviations are larger. Thus, the Price line-shape function with the first ξ correction of Westlye et al. [23,34] mainly provides superior results for the apparent total gas emissivities and the apparent gas emissivities of the 4.3 µm band. The absolute relative deviations are typically below 2% for the apparent total gas emissivities and below 1% for the apparent band gas emissivities of the 4.3 µm band. In contrast, the apparent gas emissivities of the 2.7 µm band and the 2.0 µm band are only slightly better compared to the values that were obtained using the Voigt line-shape function and the cut-off criterion.

Since the existing adjustments of the line profiles have only minor effects on the predicted spectra of both the 2.7 µm band and the 2.0 µm band and further adjustments are expected not to provide

Table 7
Losses of integrated intensity based on the LBL model with the HITEMP-2010 database, the Voigt line-shape function and the cut-off criterion of Alberti et al. [21].

$x_{CO_2,gas}$	T_{gas} / K	Loss of integrated intensity / %					
		1 bar	5 bar	10 bar	20 bar	40 bar	60 bar
0.2	773.15	−0.07	−0.25	−0.45	−0.77	−1.38	−5.84
	1273.15	−0.05	−0.17	−0.30	−0.53	−0.93	−9.43
1.0	773.15	−0.07	−0.26	−0.45	−0.80	−1.38	–
	1273.15	−0.05	−0.17	−0.30	−0.52	−0.92	–

Table 8
Relative deviations concerning the apparent total gas emissivities of CO_2 based on the LBL model with the HITRAN-2020 database and two line-shape functions. B: Voigt line-shape function with the cut-off criterion of Alberti et al. [21], C: Price line-shape function with the first ξ correction of Westlye et al. [23,34].

LSF	$x_{CO_2,gas}$	T_{gas} / K	RD_ε / %					
			1 bar	5 bar	10 bar	20 bar	40 bar	60 bar
B	0.2	773.15	−3.09	−0.18	−0.19	3.12	5.76	7.36
		1273.15	−12.59	−12.72	−14.46	−14.78	−12.47	−11.75
	1.0	773.15	−4.13	−0.17	1.77	4.14	3.38	–
		1273.15	−14.15	−15.71	−15.42	−13.08	−10.55	–
C	0.2	773.15	−3.18	−0.85	−2.01	−1.69	−2.73	−2.01
		1273.15	−12.75	−13.11	−14.97	−16.21	−16.11	−16.51
	1.0	773.15	−3.73	−2.04	−2.89	−3.34	−3.52	–
		1273.15	−14.12	−16.37	−16.93	−16.51	−16.36	–

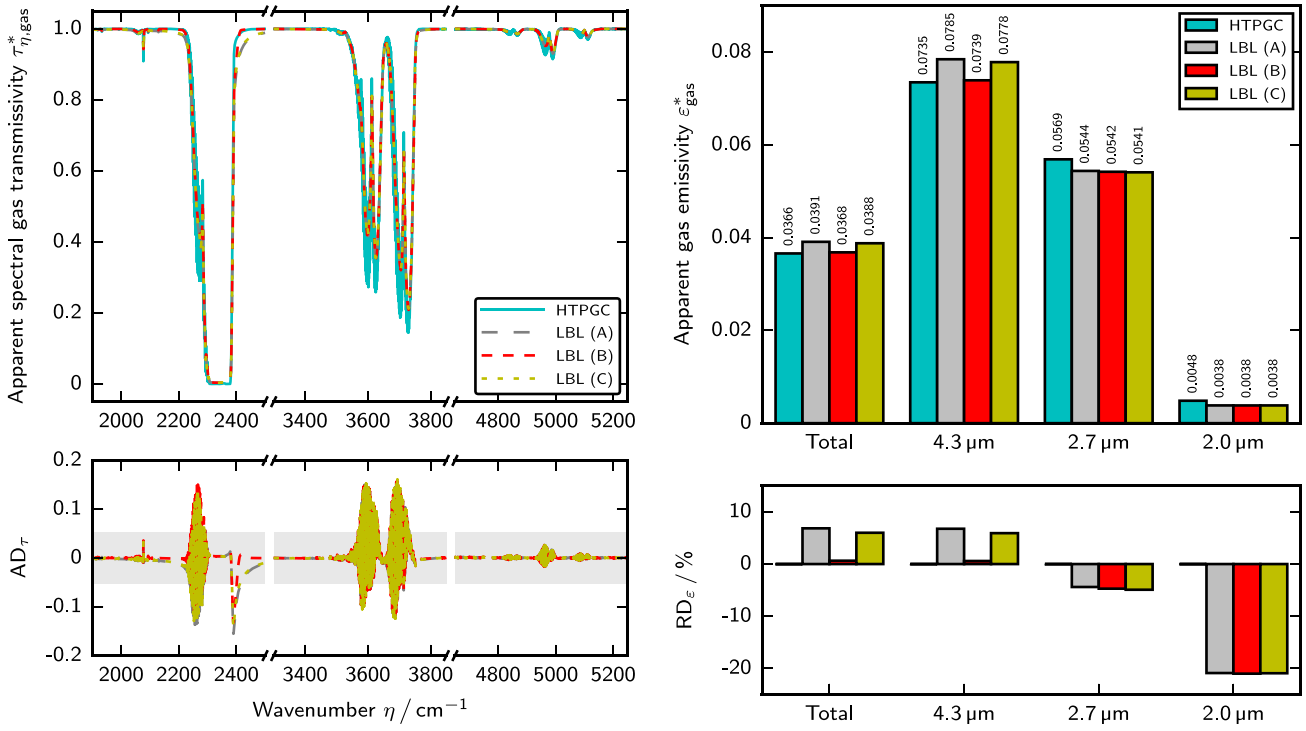

Fig. 3. Measured and predicted apparent spectral gas transmissivities (left) and measured and predicted apparent total and band gas emissivities (right) for condition 1 (100% CO_2 at 1.02 bar and 296.75 K). For details of legend, see list of acronyms.

significant improvements, the differences between the measured and predicted data for the 2.7 µm band and the 2.0 µm band are analysed below.

For 20% CO_2 and the 2.0 µm band (see results for line-shape function C in Table 6), the absolute relative deviations are significantly larger at 1273.15 K than at 773.15 K for pressures up to 10 bar, while the absolute relative deviations are similar at both 773.15 K and 1273.15 K for higher pressures. Furthermore, for 20% CO_2 and the 2.7 µm band (see results for line-shape function C in Table 5), the absolute relative deviations significantly decrease from 1 bar to 5 bar

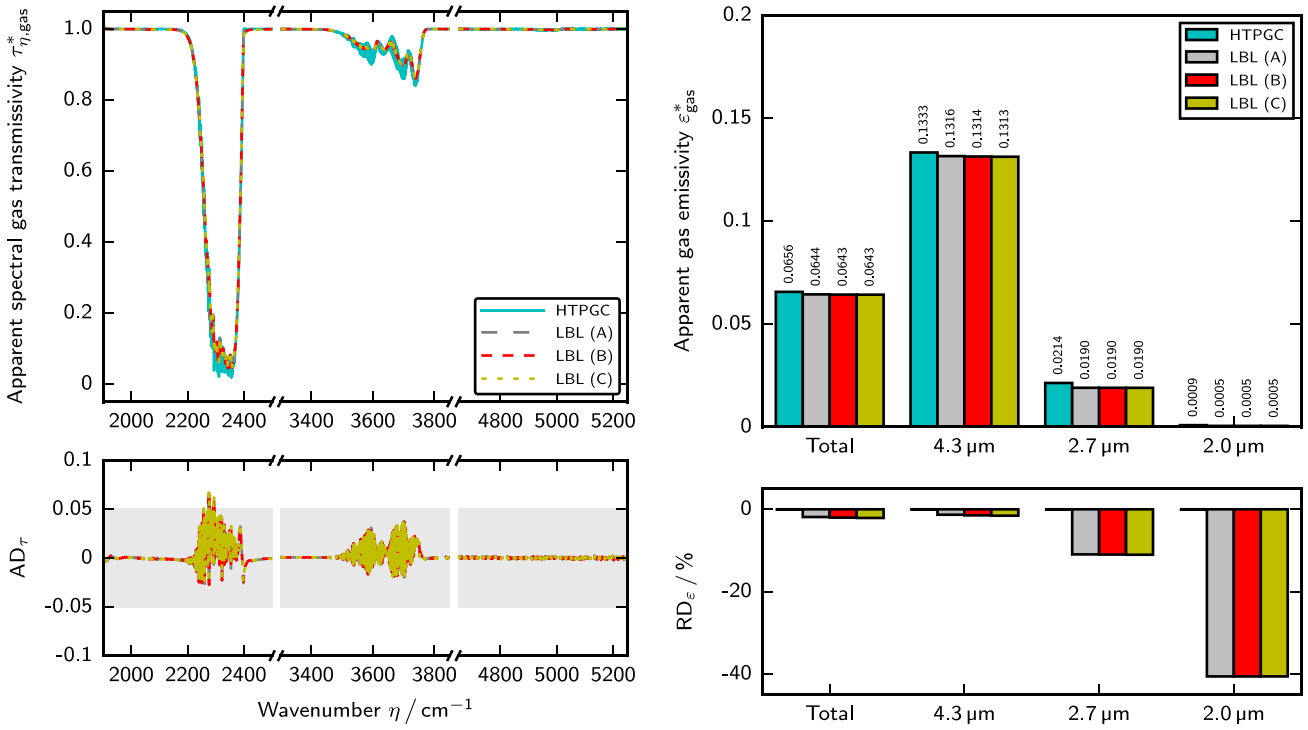

Fig. 4. Measured and predicted apparent spectral gas transmissivities (left) and measured and predicted apparent total and band gas emissivities (right) for condition 2 (20% CO_2+80% N_2 at 1.05 bar and 784.25 K). For details of legend, see list of acronyms.

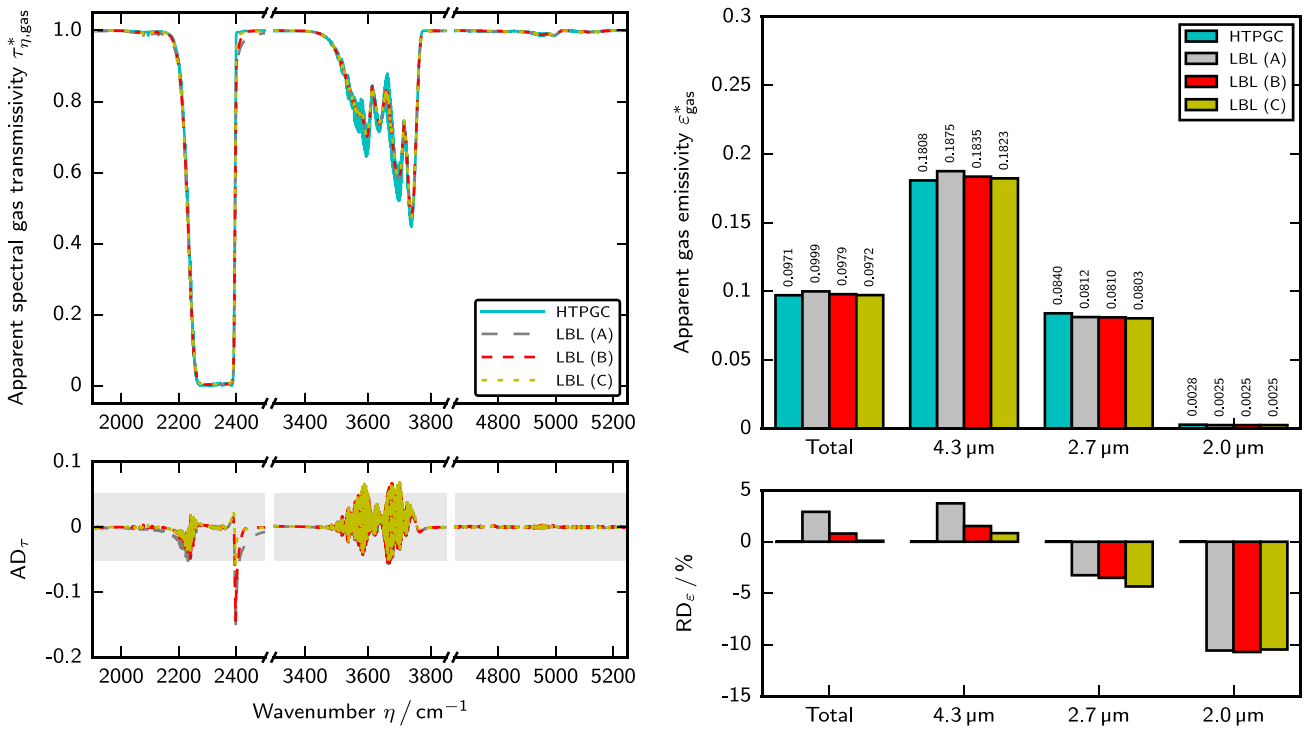

Fig. 5. Measured and predicted apparent spectral gas transmissivities (left) and measured and predicted apparent total and band gas emissivities (right) for condition 3 (20% CO_2+80% N_2 at 5.03 bar and 783.25 K). For details of legend, see list of acronyms.

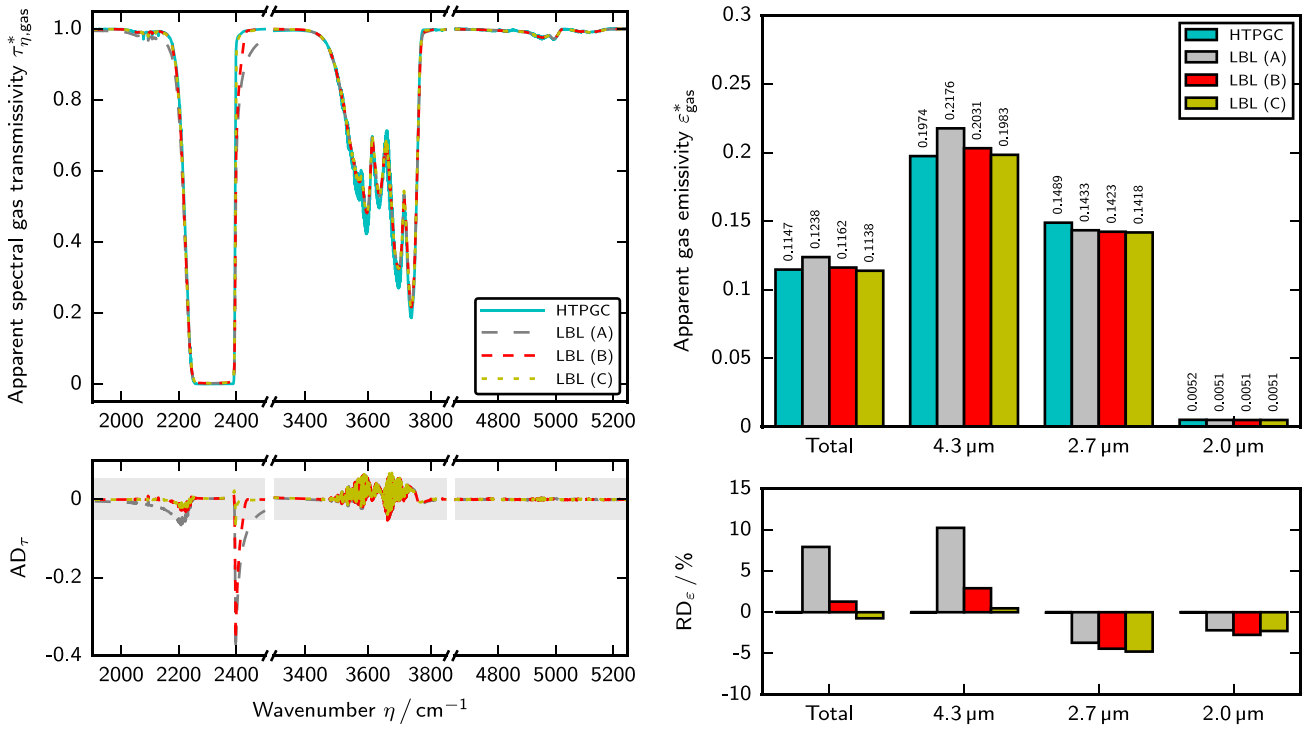

Fig. 6. Measured and predicted apparent spectral gas transmissivities (left) and measured and predicted apparent total and band gas emissivities (right) for condition 4 (20% CO_2+80% N_2 at 10.30 bar and 781.35 K). For details of legend, see list of acronyms.

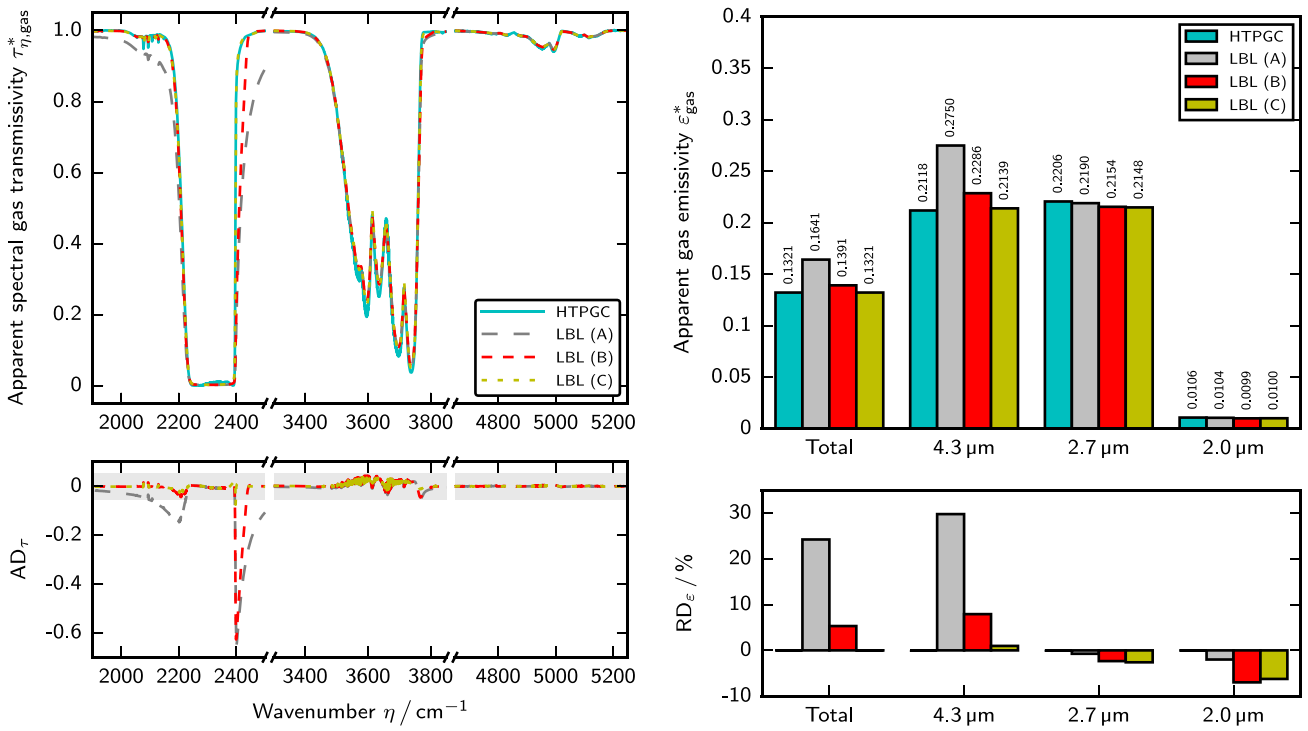

Fig. 7. Measured and predicted apparent spectral gas transmissivities (left) and measured and predicted apparent total and band gas emissivities (right) for condition 5 (20% CO_2+80% N_2 at 20.26 bar and 777.15 K). For details of legend, see list of acronyms.

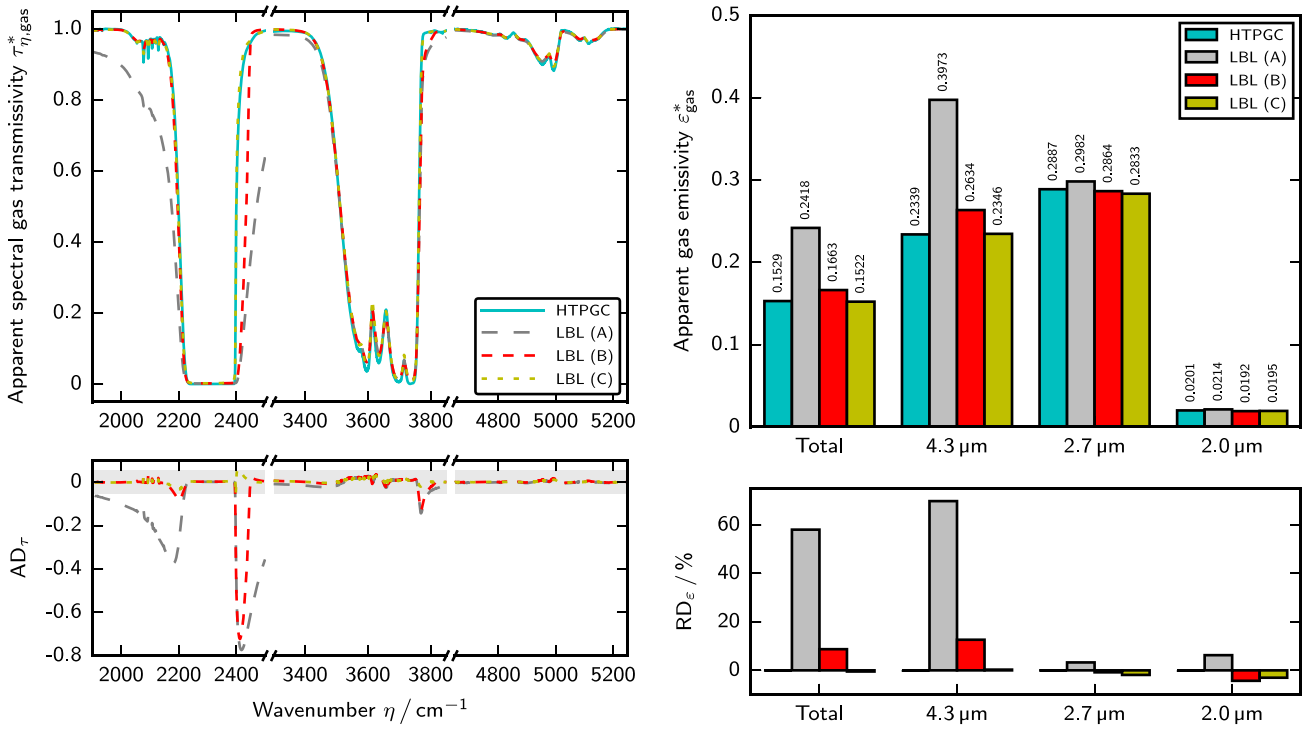

Fig. 8. Measured and predicted apparent spectral gas transmissivities (left) and measured and predicted apparent total and band gas emissivities (right) for condition 6 (20% CO_2+80% N_2 at 40.05 bar and 772.25 K). For details of legend, see list of acronyms.

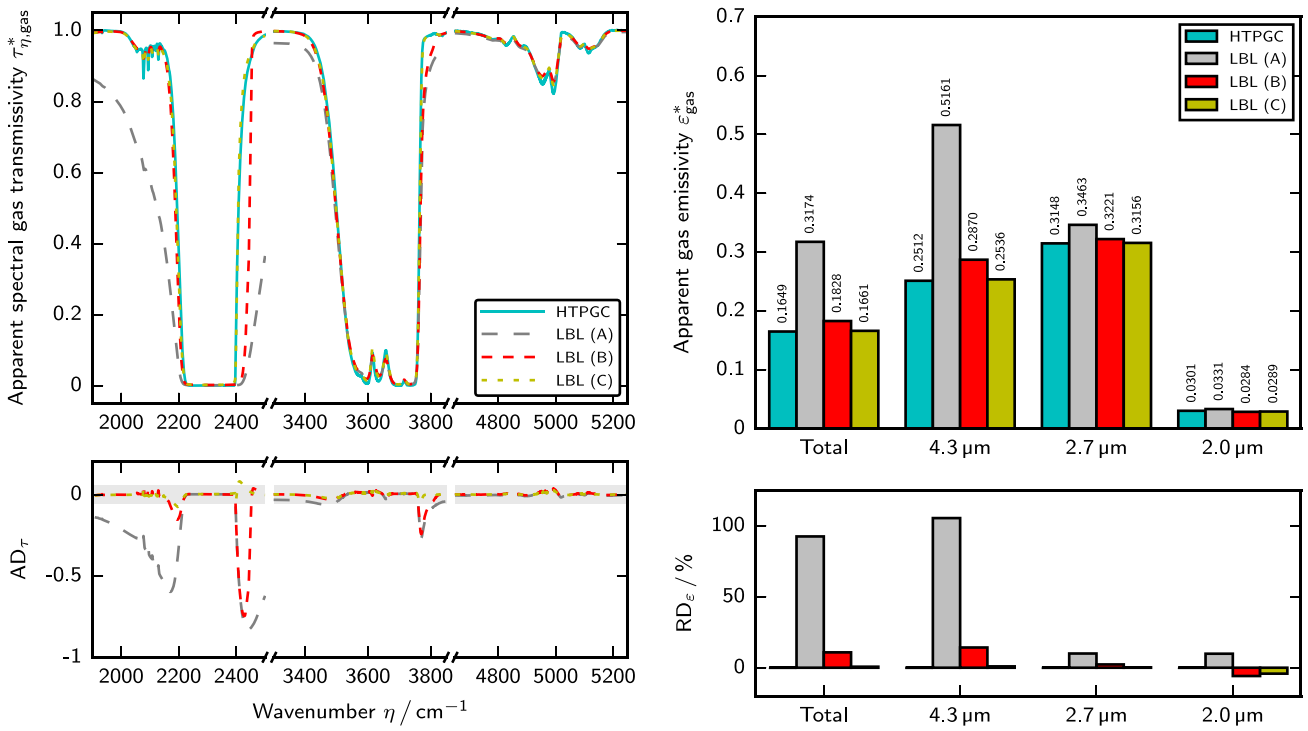

Fig. 9. Measured and predicted apparent spectral gas transmissivities (left) and measured and predicted apparent total and band gas emissivities (right) for condition 7 (20% CO_2+80% N_2 at 60.22 bar and 773.15 K). For details of legend, see list of acronyms.

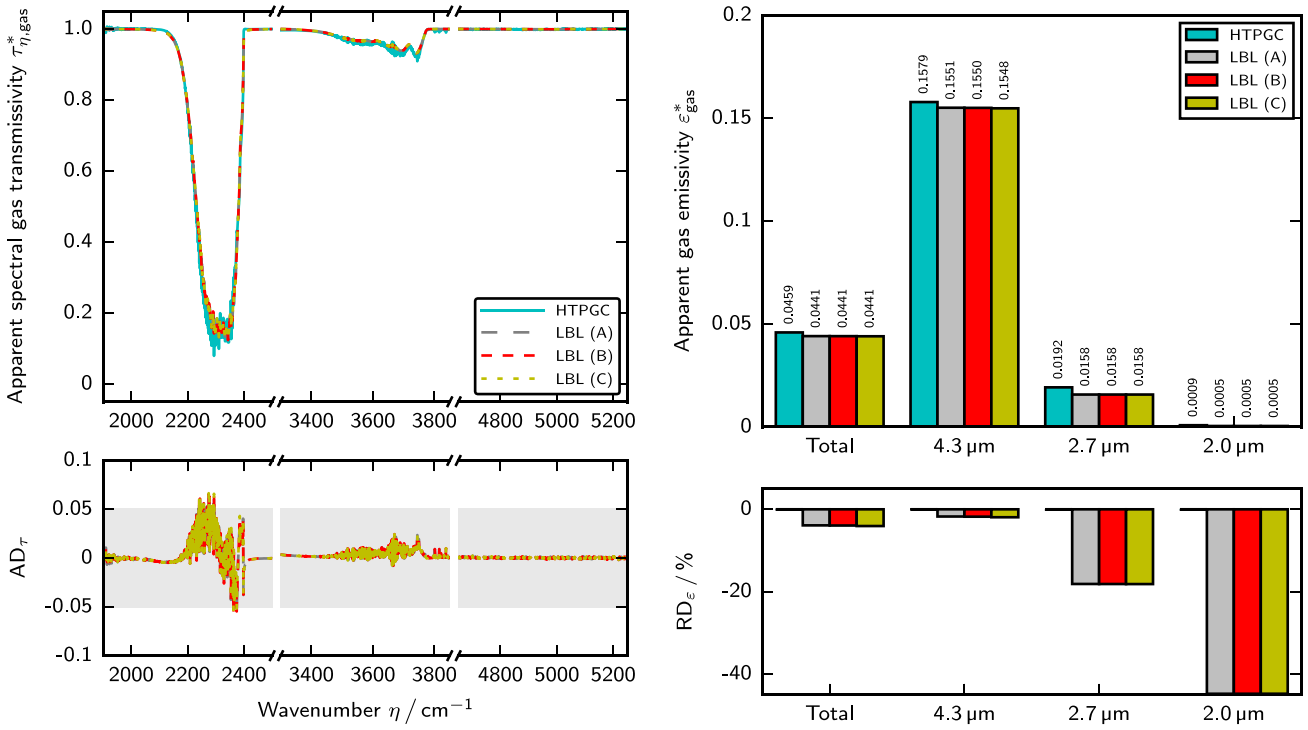

Fig. 10. Measured and predicted apparent spectral gas transmissivities (left) and measured and predicted apparent total and band gas emissivities (right) for condition 8 (20% CO_2+80% N_2 at 1.04 bar and 1281.54 K). For details of legend, see list of acronyms.

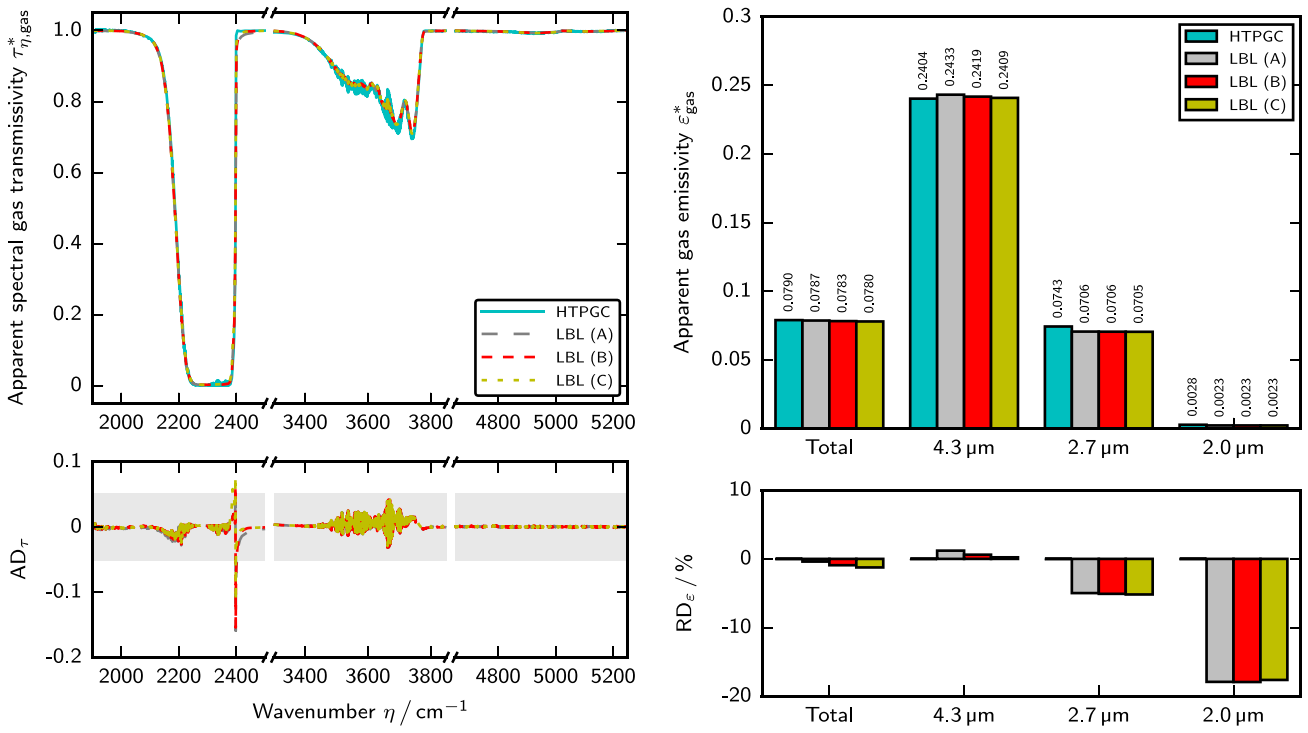

Fig. 11. Measured and predicted apparent spectral gas transmissivities (left) and measured and predicted apparent total and band gas emissivities (right) for condition 9 (20% CO_2+80% N_2 at 5.03 bar and 1280.67 K). For details of legend, see list of acronyms.

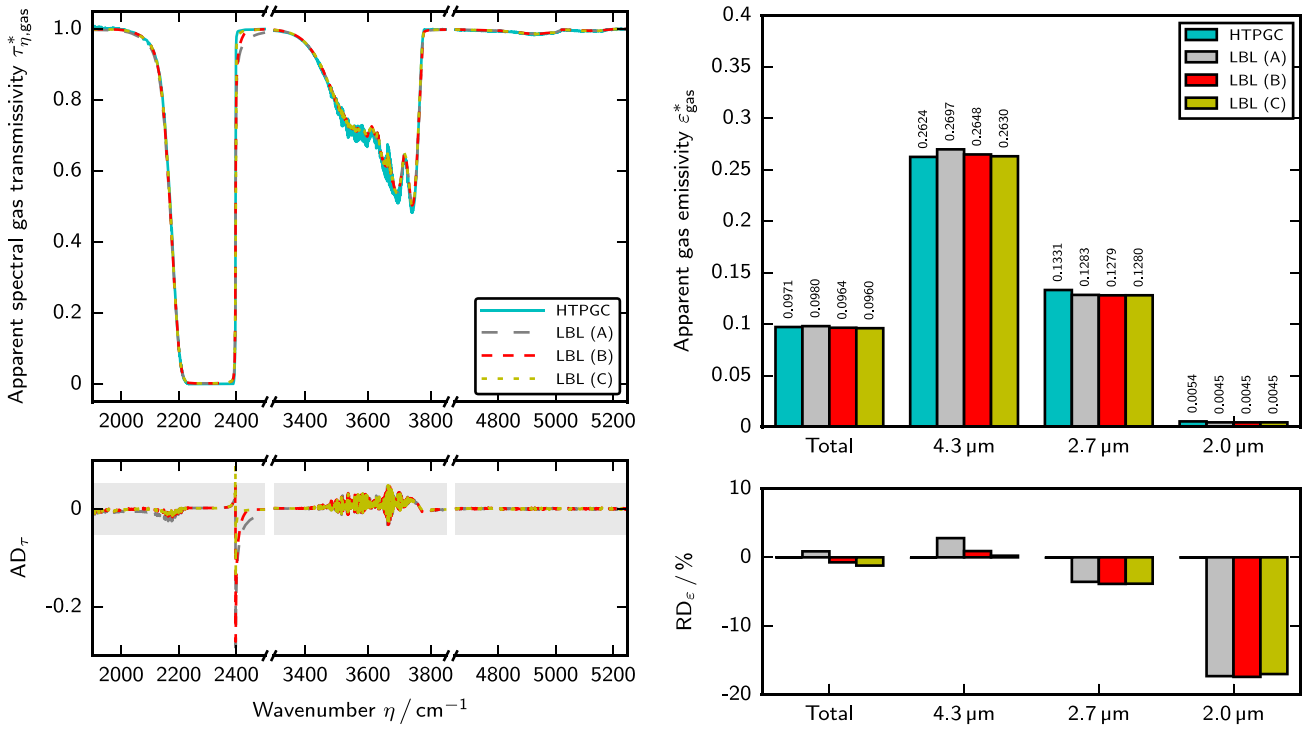

Fig. 12. Measured and predicted apparent spectral gas transmissivities (left) and measured and predicted apparent total and band gas emissivities (right) for condition 10 (20% CO_2+80% N_2 at 10.00 bar and 1276.01 K). For details of legend, see list of acronyms.

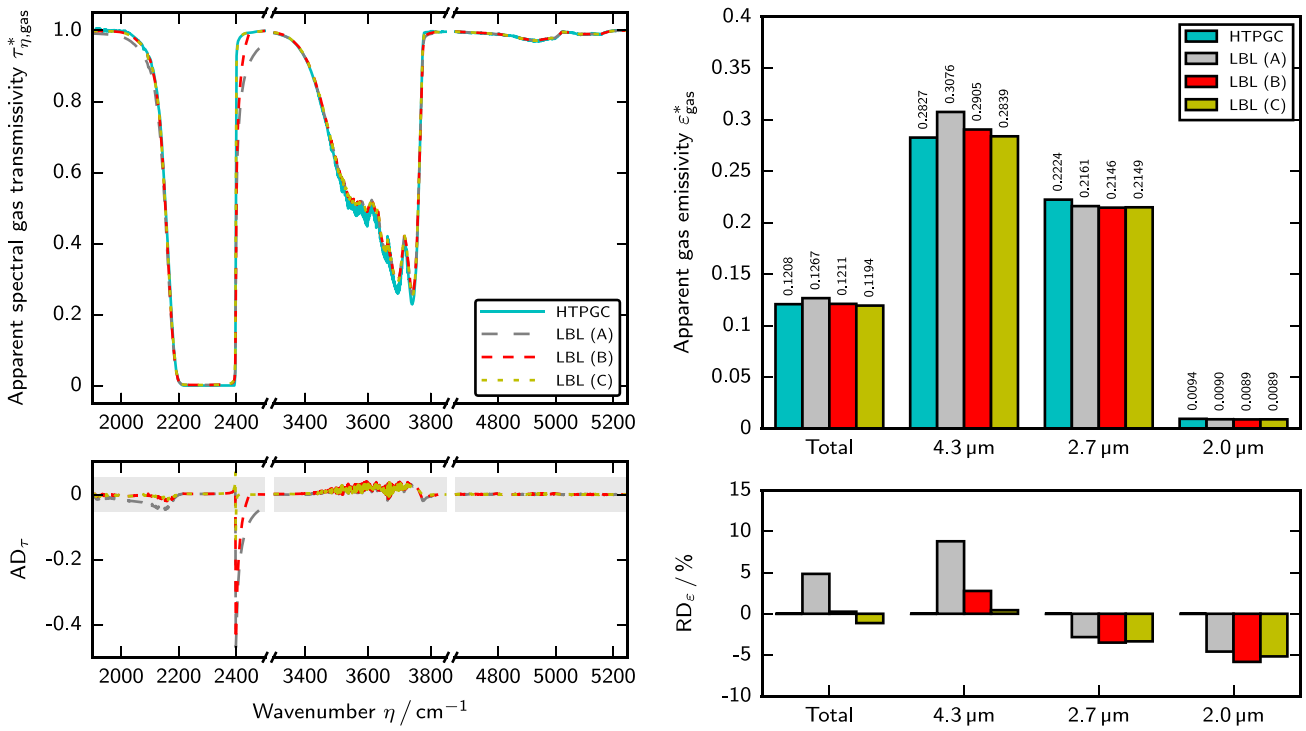

Fig. 13. Measured and predicted apparent spectral gas transmissivities (left) and measured and predicted apparent total and band gas emissivities (right) for condition 11 (20% CO_2+80% N_2 at 19.96 bar and 1275.82 K). For details of legend, see list of acronyms.

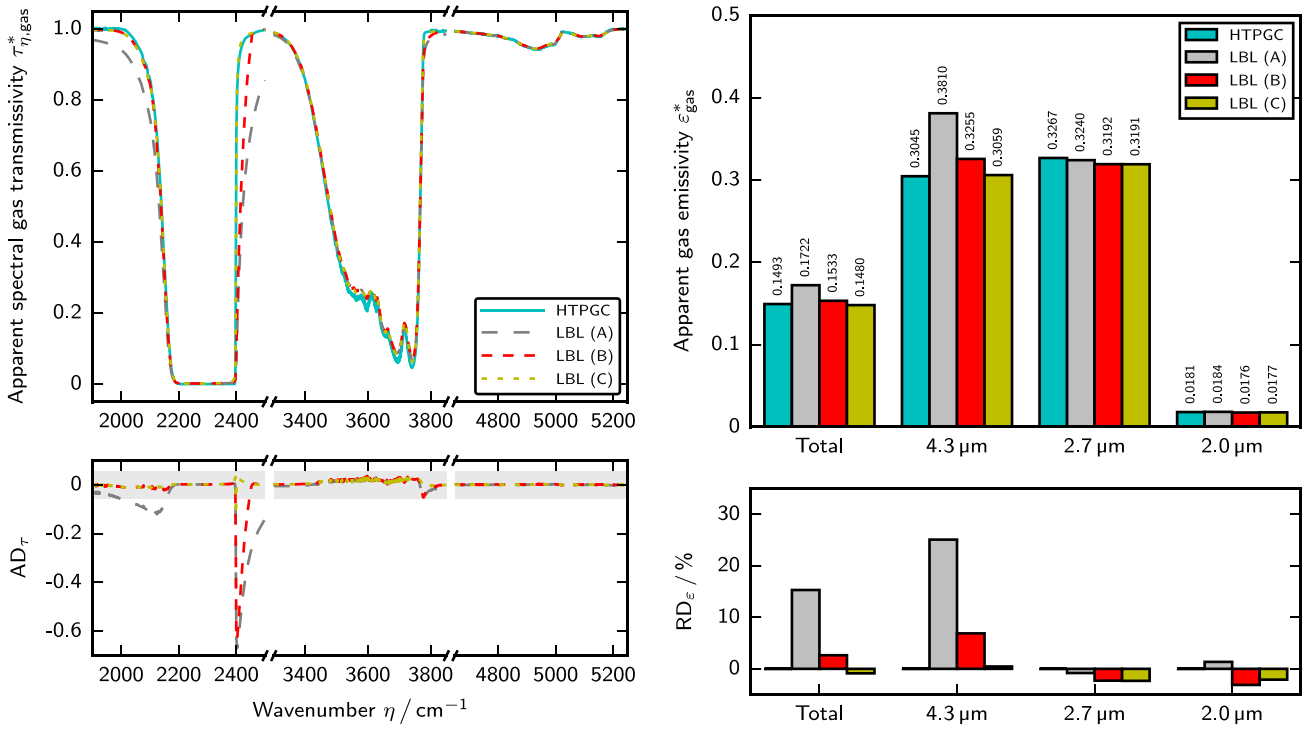

Fig. 14. Measured and predicted apparent spectral gas transmissivities (left) and measured and predicted apparent total and band gas emissivities (right) for condition 12 (20% CO_2+80% N_2 at 40.00 bar and 1265.92 K). For details of legend, see list of acronyms.

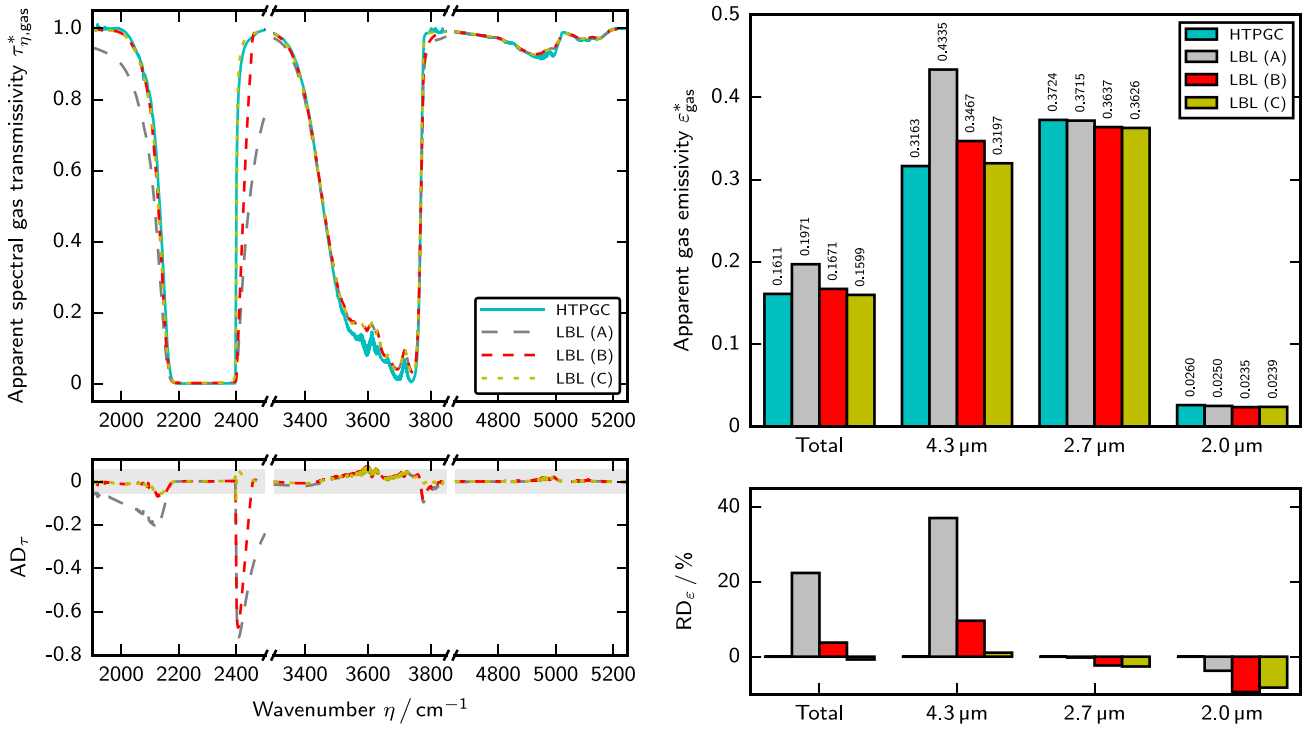

Fig. 15. Measured and predicted apparent spectral gas transmissivities (left) and measured and predicted apparent total and band gas emissivities (right) for condition 13 (20% CO_2+80% N_2 at 54.14 bar and 1280.67 K). For details of legend, see list of acronyms.

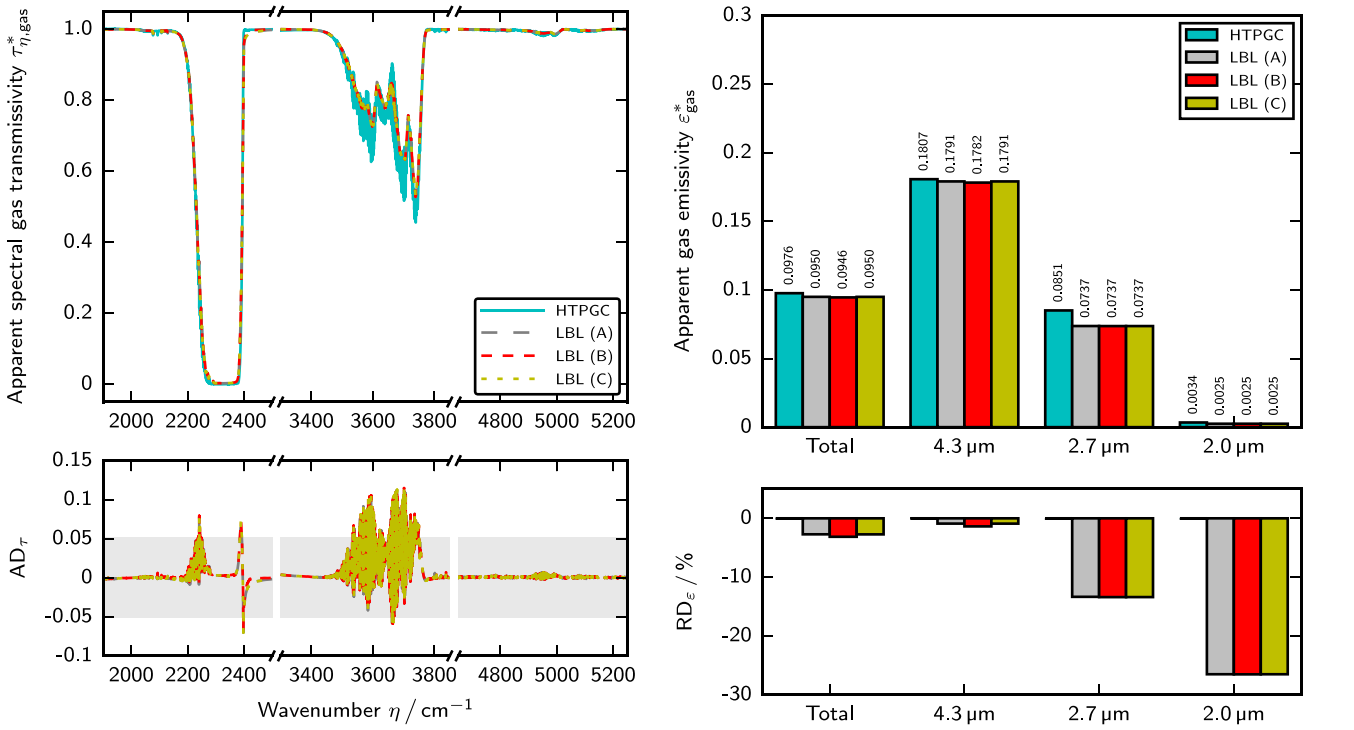

Fig. 16. Measured and predicted apparent spectral gas transmissivities (left) and measured and predicted apparent total and band gas emissivities (right) for condition 14 (100% CO_2 at 1.01 bar and 780.15 K). For details of legend, see list of acronyms.

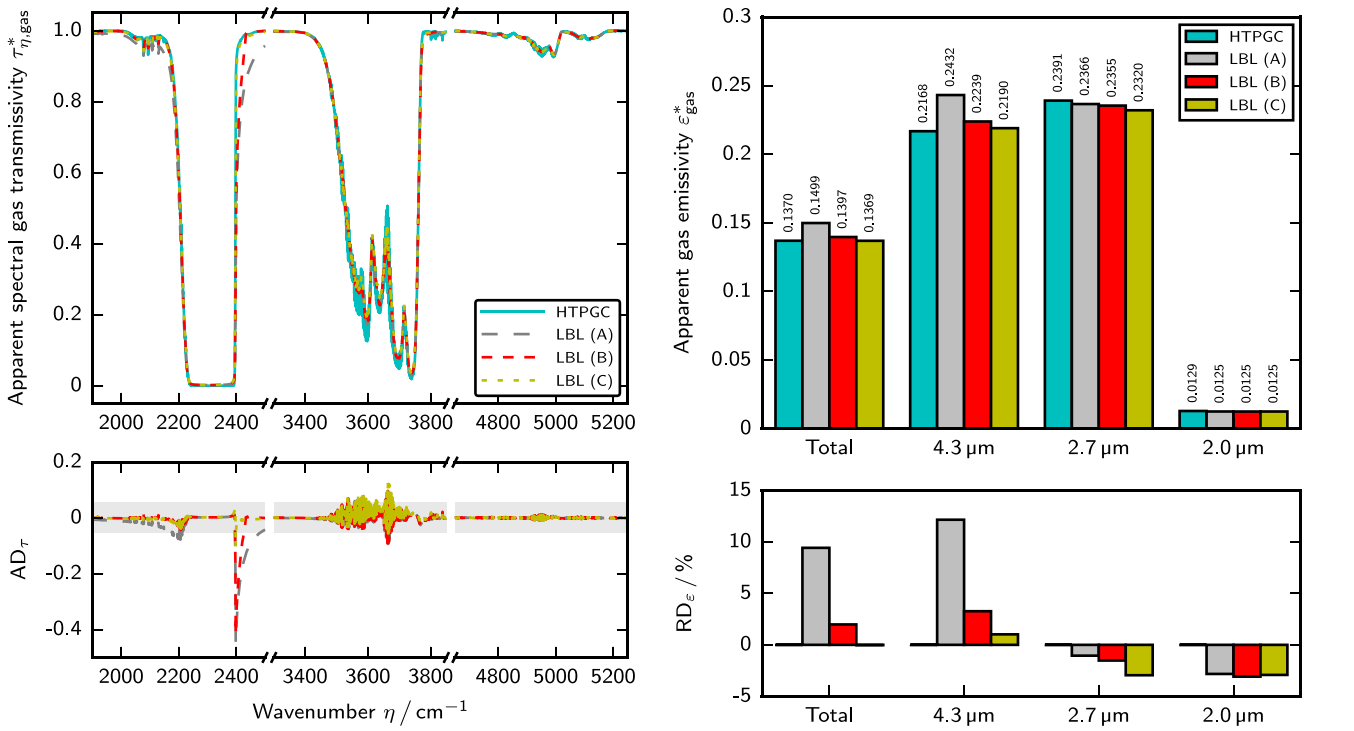

Fig. 17. Measured and predicted apparent spectral gas transmissivities (left) and measured and predicted apparent total and band gas emissivities (right) for condition 15 (100% CO_2 at 5.13 bar and 780.15 K). For details of legend, see list of acronyms.

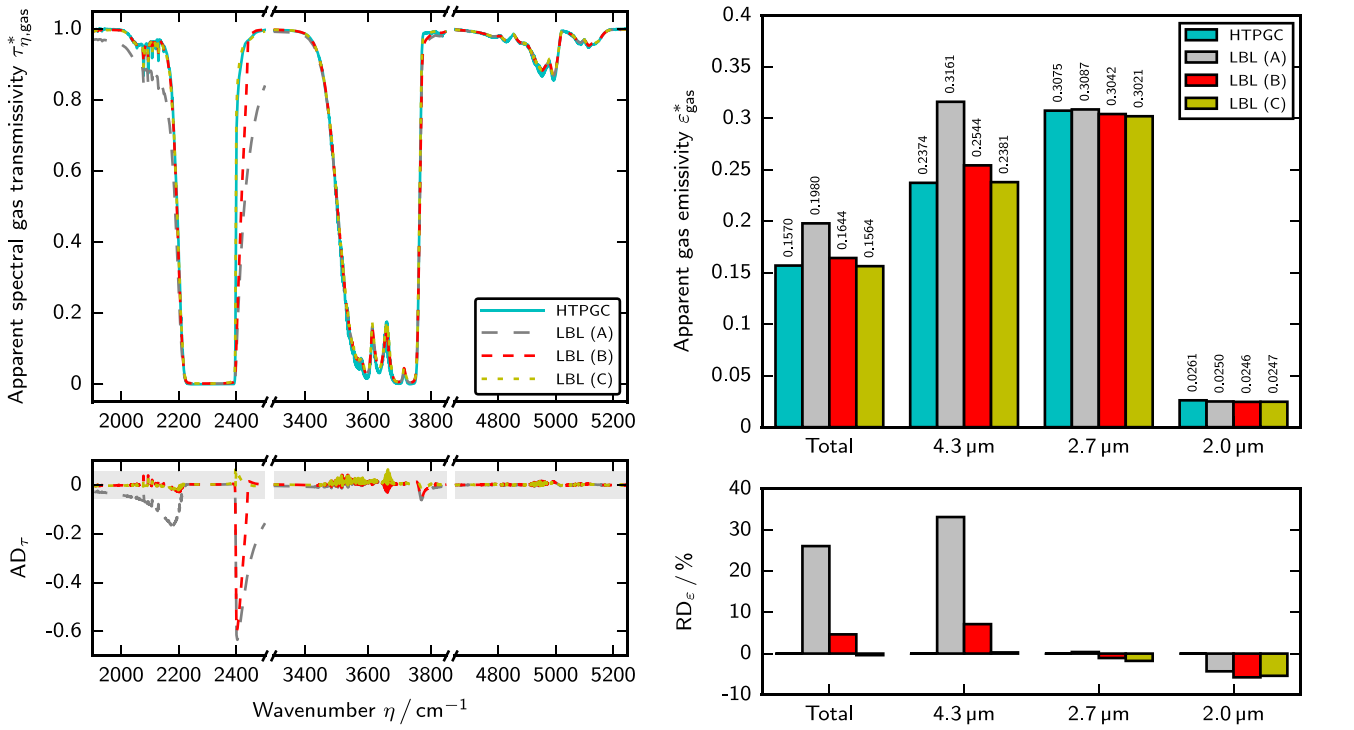

Fig. 18. Measured and predicted apparent spectral gas transmissivities (left) and measured and predicted apparent total and band gas emissivities (right) for condition 16 (100% CO_2 at 10.27 bar and 779.63 K). For details of legend, see list of acronyms.

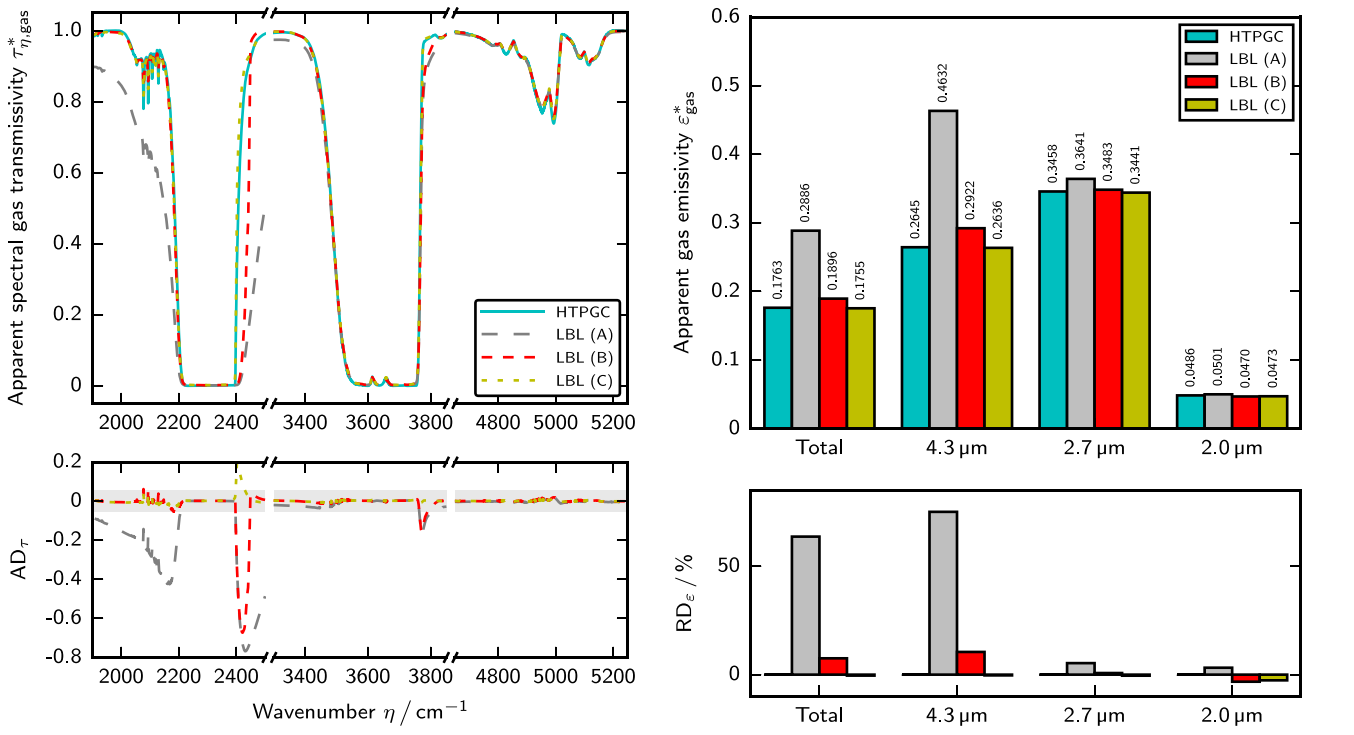

Fig. 19. Measured and predicted apparent spectral gas transmissivities (left) and measured and predicted apparent total and band gas emissivities (right) for condition 17 (100% CO_2 at 20.27 bar and 771.39 K). For details of legend, see list of acronyms.

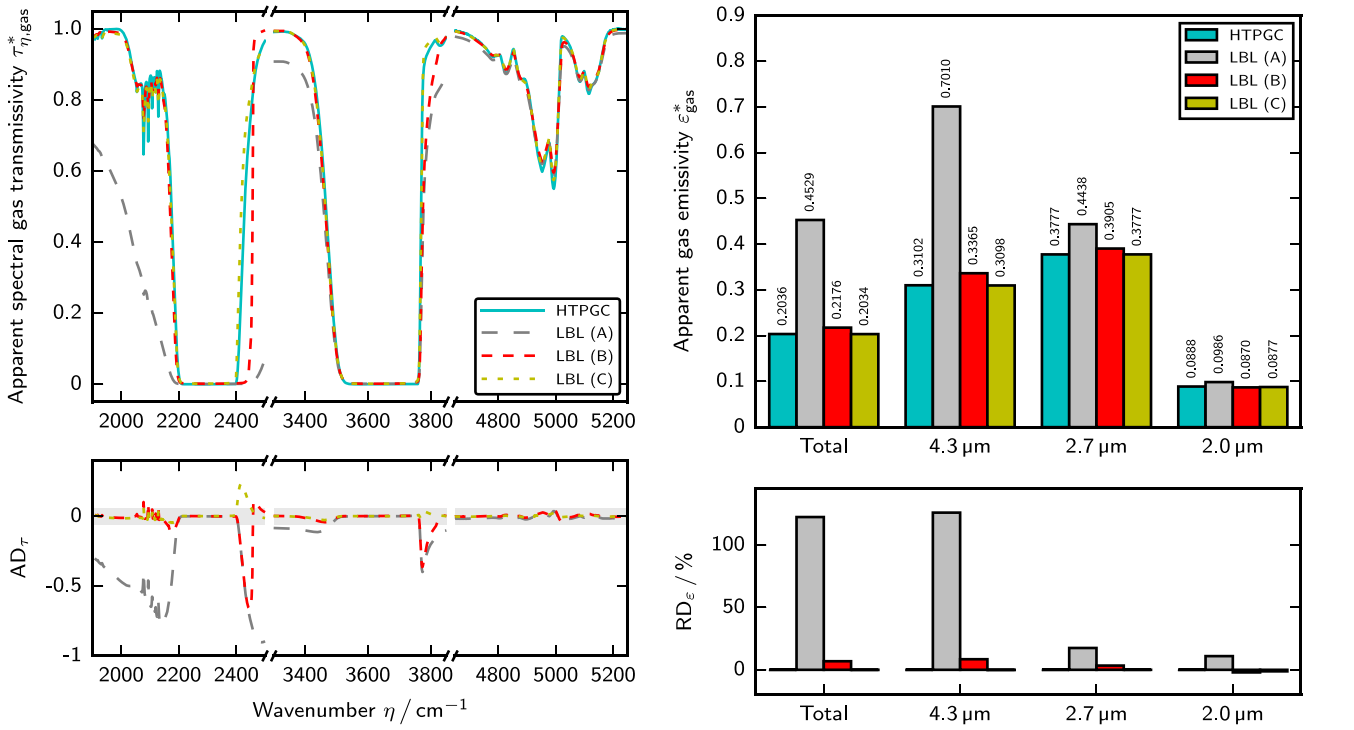

Fig. 20. Measured and predicted apparent spectral gas transmissivities (left) and measured and predicted apparent total and band gas emissivities (right) for condition 18 (100% CO_2 at 40.14 bar and 775.56 K). For details of legend, see list of acronyms.

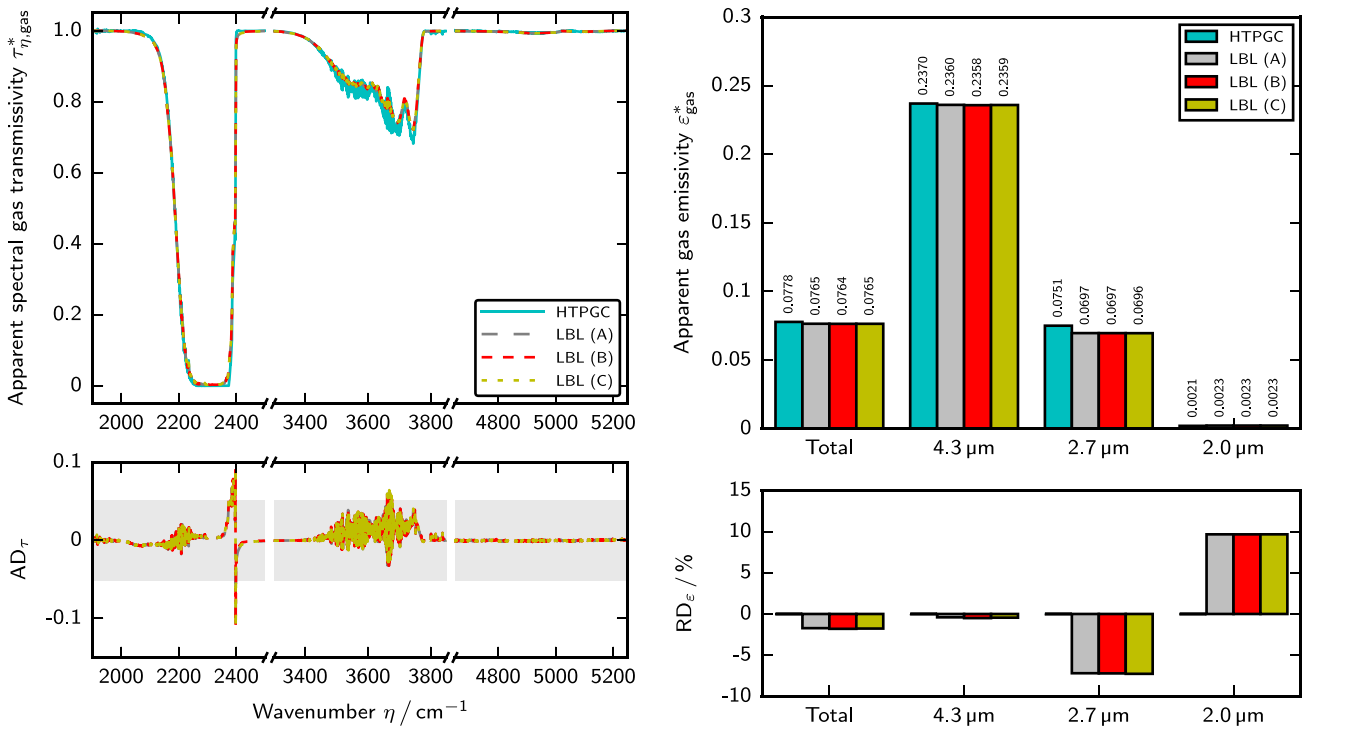

Fig. 21. Measured and predicted apparent spectral gas transmissivities (left) and measured and predicted apparent total and band gas emissivities (right) for condition 19 (100% CO_2 at 1.02 bar and 1281.54 K). For details of legend, see list of acronyms.

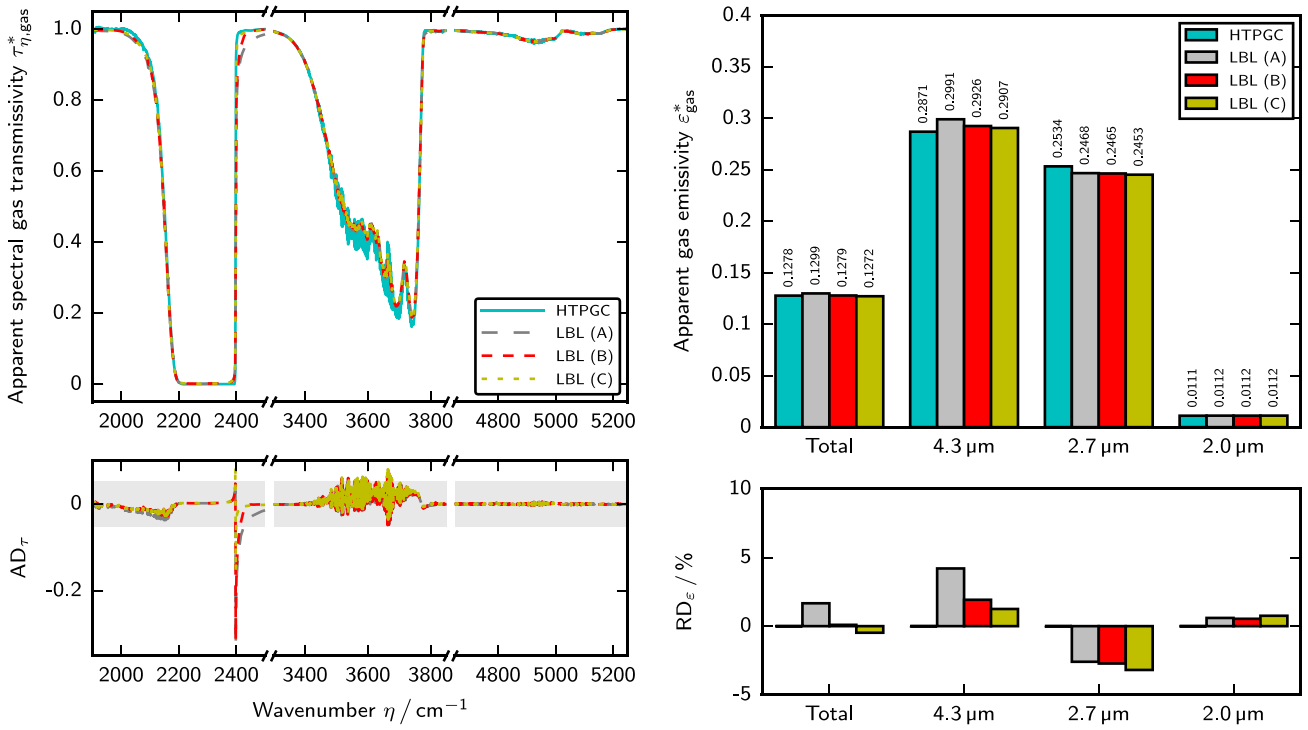

Fig. 22. Measured and predicted apparent spectral gas transmissivities (left) and measured and predicted apparent total and band gas emissivities (right) for condition 20 (100% CO_2 at 5.025 bar and 1280.67 K). For details of legend, see list of acronyms.

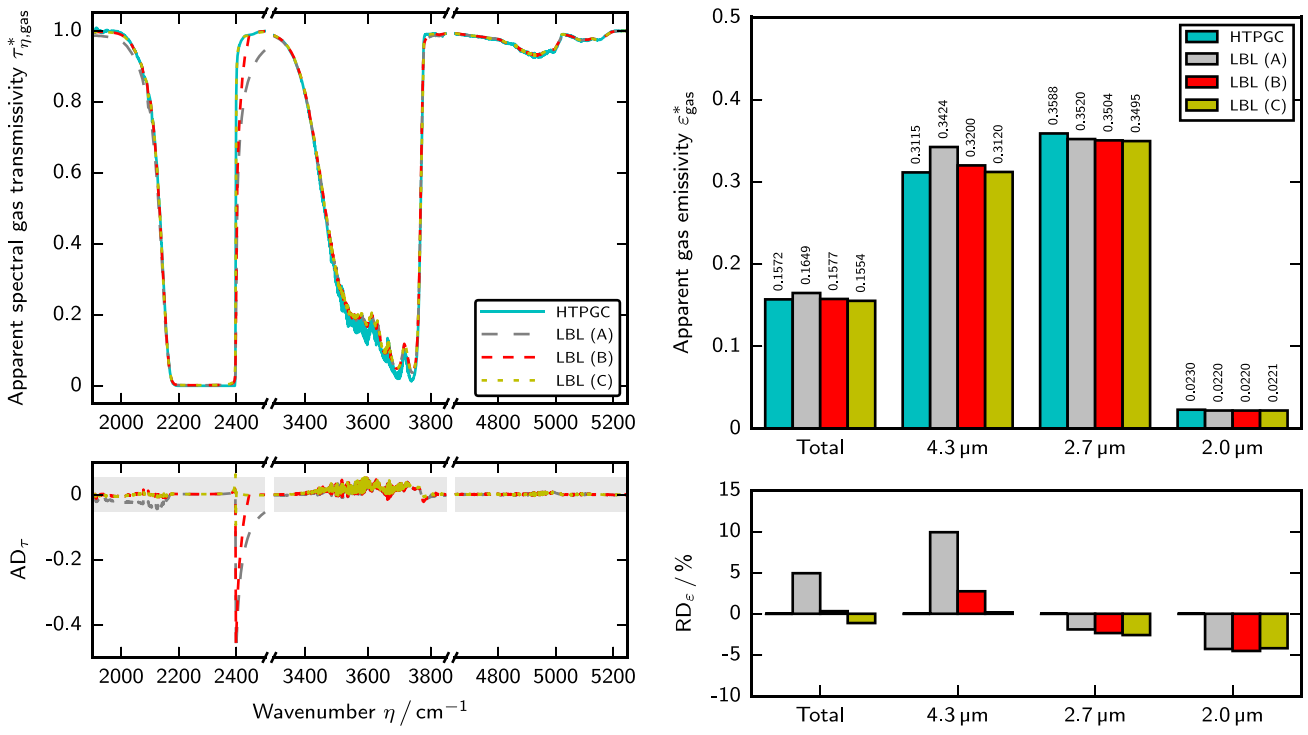

Fig. 23. Measured and predicted apparent spectral gas transmissivities (left) and measured and predicted apparent total and band gas emissivities (right) for condition 21 (100% CO_2 at 10.00 bar and 1276.01 K). For details of legend, see list of acronyms.

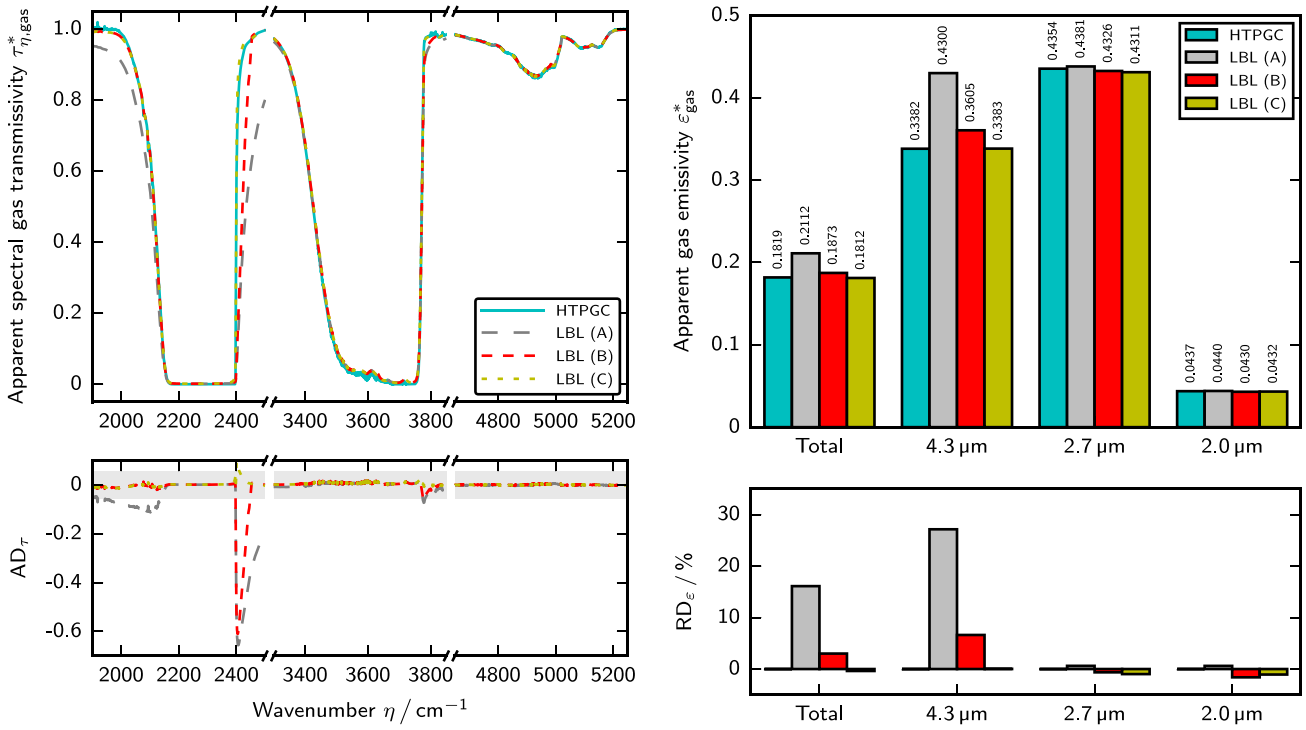

Fig. 24. Measured and predicted apparent spectral gas transmissivities (left) and measured and predicted apparent total and band gas emissivities (right) for condition 22 (100% CO_2 at 20.00 bar and 1276.01 K). For details of legend, see list of acronyms.

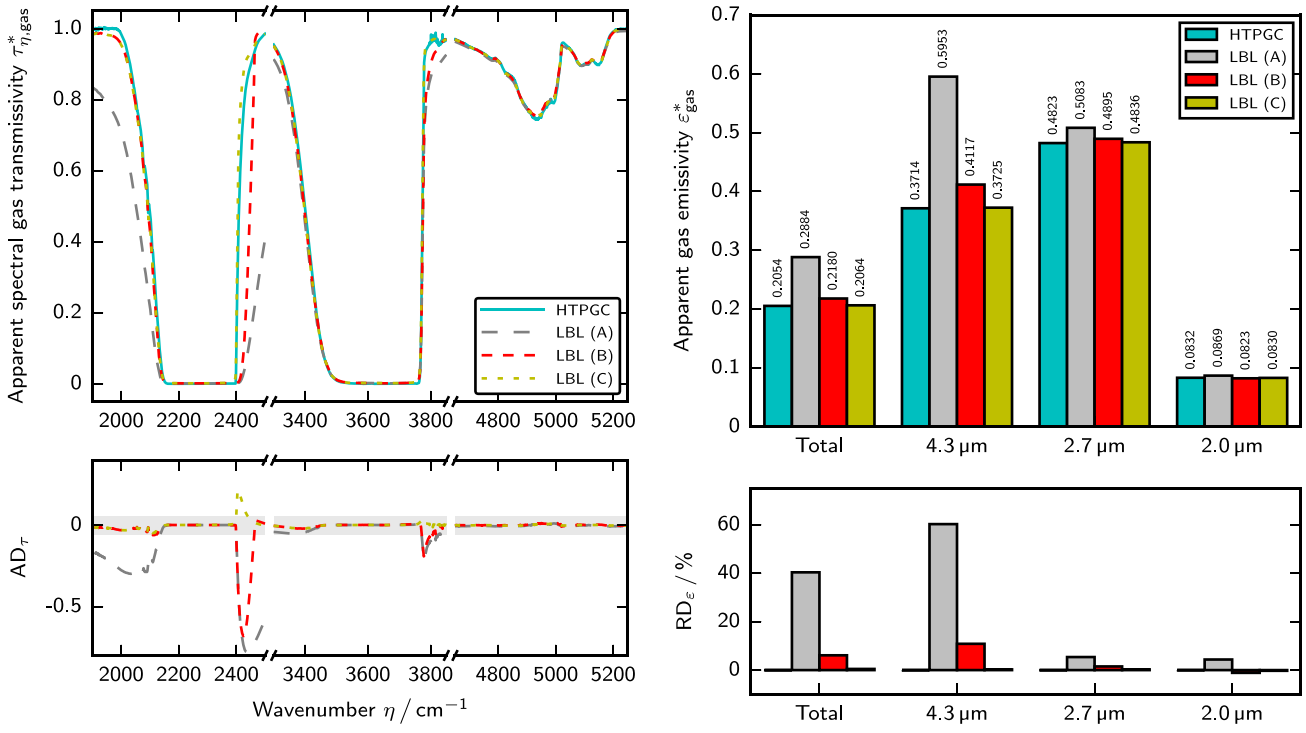

Fig. 25. Measured and predicted apparent spectral gas transmissivities (left) and measured and predicted apparent total and band gas emissivities (right) for condition 23 (100% CO_2 at 40.00 bar and 1265.92 K). For details of legend, see list of acronyms.

at both 773.15 K and 1273.15 K. These strong changes are connected with the appearance of numerous vibrational CO_2 lines. At high temperatures and high pressures, such weak lines are magnified while the strong lines contribute to the saturation of the transmissivity/emissivity spectra. While most of the strong lines in the 2.7 µm band are already in saturation for pressures above 1 bar, this effect is observed for the 2.0 µm band and 1273.15 K above 10 bar.

For 100% CO_2 and both the 2.7 µm band and the 2.0 µm band (see results for line-shape function C in Tables 5 and 6), only small differences between the measured and predicted data can be found for pressures above 5 bar. This is because the strongest lines do not contribute any more to the band gas emissivities, while the weak ones do.

Concluding, the presented measurement and modelling results show that the weak CO_2 lines in the 2.7 µm band and the 2.0 µm band have the appropriate line strengths, while the line strengths of the strong lines in the 2.7 µm band and the 2.0 µm band are systematically underestimated in the HITEMP-2010 database. This conclusion assumes that line-mixing effects can be ignored, i. e. the observed deficiency of the line strengths of the strong lines could be also attributed to line-mixing and might disappear if line-mixing effects are accounted for.

3.2.3. Lorentz line-shape function with cut-off criterion

The Voigt line-shape function was used as baseline function to account for Doppler broadening. For comparison, apparent total gas emissivities and apparent band gas emissivities were also obtained using the Lorentz line-shape function and the cut-off criterion of Alberti et al. [21]. The results show that predictions change less than 0.07% for a total gas pressure of 1 bar and less than 0.007% for total gas pressures between 5 bar and 60 bar. Thus, both the Voigt line-shape function and the Lorentz line-shape function can be applied with good accuracy in combination with the cut-off criterion of Alberti et al. [21].

3.2.4. Price line-shape function with second ξ correction

The Price line-shape function was also combined with the revised ξ correction of Westlye et al. [35]. The relative deviations concerning the apparent total gas emissivities and the apparent band gas emissivities are given in Tables 3–6 (see results for line-shape function D). The values are marked in blue and brown according to Section 3.2.2. Thus, for 20% CO_2, the Price line-shape function with the second ξ correction of Westlye et al. [35] provides superior results for the apparent gas emissivities of the 4.3 µm band compared to the Voigt line-shape function with the cut-off criterion. This in agreement with the previous validation of Westlye et al. [35] for the 4.3 µm band and the fact that the second ξ correction of Westlye et al. [35] was derived for gas conditions with smaller CO_2 concentrations, i. e. conditions that can be expected in combustion flames. However, the results are slightly inferior to the predictions based on the first ξ correction.

Furthermore, for 100% CO_2, Tables 3 and 4 (see results for line-shape function D) show less impressive results for the apparent total gas emissivity and the apparent band gas emissivity of the 4.3 µm band. This is attributable to two factors. Firstly, the Price line-shape function with the second ξ correction was used outside its validation range. Secondly, for 100% CO_2, the second ξ correction of Westlye et al. [35] reduces to $\xi = 2$. Thus, the modified Price line-shape function collapses to the Lorentz line-shape function.

Concluding, predictions using the Price line-shape function with the second ξ correction of Westlye et al. [35] are inferior to predictions relying on the Price line-shape function with the first ξ correction of Westlye et al. [23,34]. The second ξ correction of Westlye et al. [35] should only be used for gas conditions with CO_2 mole fractions of up to 20%, which rises the question why Westlye et al. [35] revised the ξ correction. First of all, Westlye et al. [35] used previous measurement data (up to 20% CO_2) for derivation and validation. Furthermore, it could be related to the fact that the Price line-shape function cannot describe well the right wing of the 4.3 µm band for 100% CO_2 with high accuracy [35]. However, the results of the previous study of Ren et al. [23] and this study show that this deficiency can be accepted for predictions at up to 1273.15 K and 40 bar.

3.2.5. Impact of gas temperature

The measured gas temperature profiles are shown for 20% CO_2 in Figs. S1-S5. Similar to previous measurements [13,20], uniform gas temperature profiles could be achieved within an accuracy of ± 10 K. However, to investigate the impact of the gas temperature accuracy on the predicted apparent gas emissivities, LBL calculations based on the Voigt line-shape function and the cut-off criterion of Alberti et al. [21] or on the Price line-shape function and the first ξ correction function of Westlye et al. [23,34] were performed using gas temperatures either increased or decreased by 10 K. The results show that the uncertainties are typically less than ± 0.5% and always less than ± 0.9% for both the apparent total gas emissivities and the apparent band gas emissivities. Thus, small temperature uncertainties within an accuracy of ± 10 K are not decisive for the accuracy of the LBL predictions.

3.2.6. Impact of spectroscopic database

The HITEMP-2010 database was used for the LBL calculations as it contains numerous additional lines at elevated temperatures compared to the HITRAN database [3]. However, LBL calculations were also carried out using the HITRAN-2020 database [40] to analyse whether the HITRAN-2020 database can better account for the strongest lines at moderate pressures than the HITEMP-2010 database and whether the higher uncertainties of the weak lines of the HITEMP-2010 database could have contributed to the erroneous predictions. The LBL calculations were performed using both standard and modified line-shape functions even though cut-off criteria and ξ corrections were developed using the HITEMP-2010 databases. The relative deviations for the apparent total gas emissivities based on the Voigt line-shape function and the cut-off criterion of Alberti et al. [21] or on the Price line-shape function and the first ξ correction function of Westlye et al. [23,34] are given in Table 8. The values are marked in blue and brown according to Section 3.2.2 and demonstrate that the apparent total gas emissivities are slightly better predicted for 20% CO_2 at 773.15 K if the Voigt line-shape function is combined with the cut-off criterion (see results for line-shape function B in Table 3). Otherwise, significantly larger deviations on an absolute basis can be observed compared to the predictions based on the HITEMP-2010 database (see results for line-shape functions B and C in Table 3).

Further comparisons of measured and calculated apparent gas emissivities of the 4.3 µm band, the 2.7 µm band and 2.0 µm band can be found in the Supplementary material (see Tables S1–S3) or are available on request.

4. Conclusions

Spectral transmissivity measurements of CO_2/N_2 mixtures at high-temperature and high-pressure conditions were combined with line-by-line calculations. The measurement data was obtained in a spectral range from 1900 cm^{-1} to 6600 cm^{-1} at gas temperatures of approximately 773 K and 1273 K and gas pressures between 1 bar and 60 bar. The measurements thus focussed on typical furnace conditions when most of the absorption lines in both the 2.7 µm band and the 2.0 µm band are saturated. The data is given in the Supplementary material and was compared with line-by-line predictions based on various line profiles.

The comparisons demonstrated that predictions of the spectral gas transmissivity, the total gas emissivity and the band gas emissivities are overall accurate if the line-by-line model is based on the Voigt line-shape function and the cut-off criterion of Alberti et al. [21] or on the Price line-shape function and the first ξ correction of Westlye

et al. [23,34]. For the Voigt line-shape function combined with the cut-off criterion, the absolute relative deviations were up to 8.8% for the apparent total gas emissivities and up to 18% for the apparent band gas emissivities above gas pressures of 5 bar. In particular, erroneous predictions were found for the right wings of the 4.3 μm band and the 2.7 μm band. For the Price line-shape function with the first ξ correction, the absolute relative deviations concerning the apparent total gas emissivities were up to 4.1% and thus significantly smaller than for the Voigt line-shape function combined with the cut-off criterion. The Price line-shape function with the first ξ correction also provided superior mathematical descriptions of the right wings of the 4.3 μm band and the 2.7 μm band and quite impressive results for the apparent band gas emissivities of the 4.3 μm band. However, similar predictions were obtained for the apparent band gas emissivities of the 2.7 μm band and the 2.0 μm band. This could indicate that the line strengths of the strong lines in both bands are systematically underestimated in the HITEMP-2010 database. However, line-mixing effects, which have not been considered in this study, may also result in enhanced absorption close to the centre of the line clusters and should be focussed in future studies, where the Price line-shape function might help to account for some of the line-mixing effects.

Furthermore, the Price line-shape function was tested with the second and most recent ξ correction of Westlye et al. [35]. This approach provided accurate results for mixtures of 20% CO_2 and 80% N_2 (in mole fractions), while inferior results were obtained for 100% CO_2. Therefore, the Price line-shape function combined with the first ξ correction should be applied in future LBL calculations at high-temperature and high-pressure conditions, while the second ξ correction should be developed further for higher CO_2 concentrations using new measurement data.

Finally, the impacts of the gas temperature accuracy and the spectroscopic database on the predictions were analysed. The comparisons showed that temperature uncertainties within an accuracy of ± 10 K are not decisive for the accuracy of the LBL predictions and that the accuracy of the LBL predictions significantly decreases when using the HITRAN-2020 database instead of the HITEMP-2010 database.

CRediT authorship contribution statement

Maximilian Dammann: Writing – review & editing, Writing – original draft, Visualisation, Validation, Software, Methodology, Investigation, Formal analysis, Conceptualisation. **Roman Weber:** Writing – review & editing, Supervision, Project administration, Funding acquisition, Conceptualisation. **Alexander Fateev:** Writing – review & editing, Validation, Project administration, Methodology, Investigation, Funding acquisition, Formal analysis. **Sønnik Clausen:** Validation, Project administration, Methodology, Investigation, Funding acquisition, Formal analysis. **Michael Alberti:** Software. **Thomas Kolb:** Supervision. **Marco Mancini:** Supervision.

Declaration of competing interest

The authors declare that they have no known competing financial interests or personal relationships that could have appeared to influence the work reported in this paper.

Data availability

Most of the data is provided in this article or the supplementary material. Further data will be made available of request.

Acknowledgements

The authors thank the Federal Ministry for Economic Affairs and Energy (BMWi) / Project Management Jülich (PtJ) for funding the project Huntorf2020 (03ET6139A). The study has also partly received funding from the European Metrology Programme for Innovation and Research (EMPIR) co-financed by the Participating States and from the European Union's Horizon 2020 research and innovation programme (Development of measurement and calibration techniques for dynamic pressures and temperatures, DynPT, 17IND07). The study was completed within the scope of the project Wasserstoffregion Nord-West-Niedersachsen (H2-ReNoWe, ZN 3773) of the Lower Saxony Ministry of Science and Culture (MWK).

Supplementary material

Supplementary material related to this article can be found online at https://doi.org/10.1016/j.jqsrt.2024.109121.

References

[1] Liu F, Consalvi J-L, Coelho PJ, Andre F, Gu M, Solovjov V, et al. The impact of radiative heat transfer in combustion processes and its modeling – with a focus on turbulent flames. Fuel 2020;281:118555. http://dx.doi.org/10.1016/j.fuel.2020.118555.

[2] Dammann M, Mancini M, Kolb T, Weber R. Thermal radiation at high-temperature and high-pressure conditions: Comparison of models for design and scale-up of entrained flow gasification processes. Therm Sci Eng Prog 2023;40:101772. http://dx.doi.org/10.1016/j.tsep.2023.101772.

[3] Rothman LS, Gordon IE, Barber RJ, Dothe H, Gamache RR, Goldman A, et al. HITEMP, the high-temperature molecular spectroscopic database. J Quant Spectrosc Radiat Transfer 2010;111(15):2139–50. http://dx.doi.org/10.1016/j.jqsrt.2010.05.001.

[4] Tashkun SA, Perevalov VI. CDSD-4000: High-resolution, high-temperature carbon dioxide spectroscopic databank. J Quant Spectrosc Radiat Transfer 2011;112(9):1403–10. http://dx.doi.org/10.1016/j.jqsrt.2011.03.005.

[5] Yurchenko SN, Mellor TM, Freedman RS, Tennyson J. ExoMol line lists – XXXIX. Ro-vibrational molecular line list for CO_2. Mon Not R Astron Soc 2020;496(4):5282–91. http://dx.doi.org/10.1093/mnras/staa1874.

[6] Huang X, Freedman RS, Tashkun S, Schwenke DW, Lee TJ. AI-3000K: Infrared line list for hot CO_2. J Mol Spectrosc 2023;392:111748. http://dx.doi.org/10.1016/j.jms.2023.111748.

[7] Scutaru D, Rosenmann L, Taine J, Wattson RB, Rothman LS. Measurements and calculations of CO_2 absorption at high temperature in the 4.3 and 2.7 μm regions. J Quant Spectrosc Radiat Transfer 1993;50(2):179–91. http://dx.doi.org/10.1016/0022-4073(93)90116-y.

[8] Modest MF, Bharadwaj SP. Medium resolution transmission measurements of CO_2 at high temperature. J Quant Spectrosc Radiat Transfer 2002;73(2–5):329–38. http://dx.doi.org/10.1016/s0022-4073(01)00219-9.

[9] Bharadwaj SP, Modest MF. Medium resolution transmission measurements of CO_2 at high temperature – an update. J Quant Spectrosc Radiat Transfer 2007;103(1):146–55. http://dx.doi.org/10.1016/j.jqsrt.2006.05.011.

[10] Tanaka T, Fukabori M, Sugita T, Yokota T, Kumazawa R, Watanabe T, et al. Line shape of the far-wing beyond the band head of the CO_2 ν_3 band. J Mol Spectrosc 2008;252(2):185–9. http://dx.doi.org/10.1016/j.jms.2008.08.004.

[11] Becher V, Clausen S, Fateev A, Spliethoff H. Validation of spectral gas radiation models under oxyfuel conditions. Part A: Gas cell experiments. Int J Greenh Gas Control 2011;5:S76–99. http://dx.doi.org/10.1016/j.ijggc.2011.05.005.

[12] Evseev V, Fateev A, Clausen S. High-resolution transmission measurements of CO_2 at high temperatures for industrial applications. J Quant Spectrosc Radiat Transfer 2012;113(17):2222–33. http://dx.doi.org/10.1016/j.jqsrt.2012.07.015.

[13] Alberti M, Weber R, Mancini M, Fateev A, Clausen S. Validation of HITEMP-2010 for carbon dioxide and water vapour at high temperatures and atmospheric pressures in 450-7600 cm^{-1} spectral range. J Quant Spectrosc Radiat Transfer 2015;157:14–33. http://dx.doi.org/10.1016/j.jqsrt.2015.01.016.

[14] Fukabori M, Nakazawa T, Tanaka M. Absorption properties of infrared active gases at high pressures. I. CO_2. J Quant Spectrosc Radiat Transfer 1986;36(3):265–70. http://dx.doi.org/10.1016/0022-4073(86)90074-9.

[15] Hartmann J-M, Perrin M-Y. CO_2 absorption beyond the ν_3 bandhead at high temperature. Appl Opt 1989;28(13):2550–3. http://dx.doi.org/10.1364/AO.28.002550.

[16] Perrin MY, Hartmann JM. Temperature-dependent measurements and modeling of absorption by CO_2-N_2 mixtures in the far line-wings of the 4.3 μm CO_2 band. J Quant Spectrosc Radiat Transfer 1989;42(4):311–7. http://dx.doi.org/10.1016/0022-4073(89)90077-0.

[17] Farooq A, Jeffries JB, Hanson RK. High-pressure measurements of CO_2 absorption near 2.7 μm: Line mixing and finite duration collision effects. J Quant Spectrosc Radiat Transf 2010;111(7-8):949–60. http://dx.doi.org/10.1016/j.jqsrt.2010.01.001.

[18] Tran H, Boulet C, Stefani S, Snels M, Piccioni G. Measurements and modelling of high pressure pure CO_2 spectra from 750 to 8500 cm^{-1}. I. Central and wing regions of the allowed vibrational bands. J Quant Spectrosc Radiat Transf 2011;112(6):925–36. http://dx.doi.org/10.1016/j.jqsrt.2010.11.021.

[19] Stefani S, Piccioni G, Snels M, Grassi D, Adriani A. CO_2 absorption coefficients at high pressure and high temperature. J Quant Spectrosc Radiat Transfer 2013;117:21–8. http://dx.doi.org/10.1016/j.jqsrt.2012.11.019.

[20] Christiansen C, Stolberg-Rohr T, Fateev A, Clausen S. High temperature and high pressure gas cell for quantitative spectroscopic measurements. J Quant Spectrosc Radiat Transfer 2016;169:96–103. http://dx.doi.org/10.1016/j.jqsrt.2015.10.006.

[21] Alberti M, Weber R, Mancini M. Re-creating Hottel's emissivity charts for carbon dioxide and extending them to 40 bar pressure using HITEMP-2010 data base. Combust Flame 2015;162(3):597–612. http://dx.doi.org/10.1016/j.combustflame.2014.09.005.

[22] Hartmann JM, Perrin MY, Ma Q, Tippings RH. The infrared continuum of pure water vapor: Calculations and high-temperature measurements. J Quant Spectrosc Radiat Transfer 1993;49(6):675–91. http://dx.doi.org/10.1016/0022-4073(93)90010-f.

[23] Ren T, Han Y, Modest MF, Fateev A, Clausen S. Evaluation of spectral line mixing models and the effects on high pressure radiative heat transfer calculations. J Quant Spectrosc Radiat Transfer 2023;302:108555. http://dx.doi.org/10.1016/j.jqsrt.2023.108555.

[24] Brodbeck C, Bouanich JP, Van-Thanh N, Hartmann JM, Khalil B, Doucen RL. Absorption of radiation by gases from low to high pressures. II. Measurements and calculations of CO infrared spectra. J Phys II 1994;4(12):2101–18. http://dx.doi.org/10.1051/jp2:1994249.

[25] Niro F, Jucks K, Hartmann J-M. Spectra calculations in central and wing regions of IR bands. IV: Software and database for the computation of atmospheric spectra. J Quant Spectrosc Radiat Transf 2005;95(4):469–81. http://dx.doi.org/10.1016/j.jqsrt.2004.11.011.

[26] Lamouroux J, Tran H, Laraia AL, Gamache RR, Rothman LS, Gordon IE, Hartmann J-M. Updated database plus software for line-mixing in CO_2 infrared spectra and their test using laboratory spectra in the 1.5-2.3 μm region. J Quant Spectrosc Radiat Transf 2010;111(15):2321–31. http://dx.doi.org/10.1016/j.jqsrt.2010.03.006.

[27] Alberti M, Weber R, Mancini M. Re-creating Hottel's emissivity charts for water vapor and extending them to 40 bar pressure using HITEMP-2010 data base. Combust Flame 2016;169:141–53. http://dx.doi.org/10.1016/j.combustflame.2016.04.013.

[28] Alberti M, Weber R, Mancini M. Absorption of infrared radiation by carbon monoxide at elevated temperatures and pressures. Part A: Advancing the line-by-line procedure based on HITEMP-2010. J Quant Spectrosc Radiat Transf 2017;200:258–71. http://dx.doi.org/10.1016/j.jqsrt.2017.05.024.

[29] Alberti M, Weber R, Mancini M. Absorption of infrared radiation by carbon monoxide at elevated temperatures and pressures. Part B: Total emissivity charts and correlations. J Quant Spectrosc Radiat Transf 2017;200:272–9. http://dx.doi.org/10.1016/j.jqsrt.2017.05.034.

[30] Alberti M, Weber R, Mancini M. Gray gas emissivities for H_2O-CO_2-CO-N_2 mixtures. J Quant Spectrosc Radiat Transfer 2018;219:274–91. http://dx.doi.org/10.1016/j.jqsrt.2018.08.008.

[31] Alberti M. Total emissivity charts for H_2O, CO_2 and CO from low to high pressures [Ph.D. Thesis], Clausthal-Zellerfeld, Germany: Fakultät für Energie- und Wirtschaftswissenschaften, Technische Universität Clausthal; 2018.

[32] Fukabori M, Nakazawa T, Tanaka M. Absorption properties of infrared active gases at high pressures. II. N_2O and CO. J Quant Spectrosc Radiat Transfer 1986;36(4):283–7. http://dx.doi.org/10.1016/0022-4073(86)90051-8.

[33] Thomas ME. Infrared- and millimeter-wavelength continuum absorption in the atmospheric windows: Measurements and models. Infrared Phys 1990;30(2):161–74. http://dx.doi.org/10.1016/0020-0891(90)90027-s.

[34] Hartz BAK. RadISpeC. Radiation interface for Matlab spectroscopy calculations. Documentation. Release 5.5.1, 2019. http://dx.doi.org/10.6084/m9.figshare.6988997.v8.

[35] Westlye FR, Hartz BAK, Ivarsson A, Fateev A, Clausen S. Evaluation of spectral radiative properties of gases in high-pressure combustion. J Quant Spectrosc Radiat Transfer 2022;280:108089. http://dx.doi.org/10.1016/j.jqsrt.2022.108089.

[36] Price DC. Empirical lineshape for computer fitting of spectral data. Aust J Phys 1981;34:51–6. http://dx.doi.org/10.1071/PH810051.

[37] Hashemi R, Gordon IE, Tran H, Kochanov RV, Karlovets EV, Tan Y, et al. Revising the line-shape parameters for air- and self-broadened CO_2 lines toward a sub-percent accuracy level. J Quant Spectrosc Radiat Transfer 2020;256:107283. http://dx.doi.org/10.1016/j.jqsrt.2020.107283.

[38] Hartmann J-M, Boulet C, Robert D. Collisional effects on molecular spectra: Laboratory experiments and models, consequences for applications. Dordrecht, The Netherlands [et al.]: Elsevier Science & Technology Books; 2008, http://dx.doi.org/10.1016/B978-0-444-52017-3.X0001-5.

[39] Lamouroux J, Régalia L, Thomas X, Vander Auwera J, Gamache RR, Hartmann J-M. CO_2 line-mixing database and software update and its tests in the 2.1 μm and 4.3 μm regions. J Quant Spectrosc Radiat Transf 2015;151:88–96. http://dx.doi.org/10.1016/j.jqsrt.2014.09.017.

[40] Gordon IE, Rothman LS, Hargreaves RJ, Hashemi R, Karlovets EV, Skinner FM, et al. The HITRAN2020 molecular spectroscopic database. J Quant Spectrosc Radiat Transfer 2022;277:107949. http://dx.doi.org/10.1016/j.jqsrt.2021.107949.